Single cell analyses reveal distinct adaptation of typhoidal and non-typhoidal *Salmonella enterica* serovars to intracellular lifestyle

Tatjana Reuter[1], Felix Scharte[1], Rico Franzkoch[1, 2], Viktoria Liss[1, 2] and Michael Hensel[1, 3]

[1]Abt. Mikrobiologie, [2]iBiOs – integrated Bioimaging Facility Osnabrück, [3]CellNanOs – Center of Cellular Nanoanalytics Osnabrück, Universität Osnabrück, Osnabrück, Germany

ORCID: 0000-0001-9948-9560, TR; 0000-0002-6710-9524, FS; 0000-0002-1304-2512, VL; 0000-0001-6604-6253, MH.

Running title: Typhoidal *Salmonella* single cell analyses

Keywords: intracellular lifestyle, typhoidal fever, *Salmonella*-containing vacuole, fluorescent protein reporter, correlative light and electron microscopy

Address for correspondence:

Michael Hensel

Abteilung Mikrobiologie

Fachbereich Biologie/Chemie, Universität Osnabrück

Barbarastr. 11

49076 Osnabrück, Germany

Tel: ++ 49 (0)541 969 3940

E-mail: Michael.Hensel@uni-osnabrueck.de

Abstract

Salmonella enterica is a common foodborne, facultative intracellular enteropathogen. Human-restricted typhoidal *S. enterica* serovars Typhi (STY) or Paratyphi A (SPA) cause severe typhoid or paratyphoid fever, while *S. enterica* serovar Typhimurium (STM) has a broad host range and in human hosts usually lead to a self-limiting gastroenteritis. Due to restriction of STY and SPA to primate hosts, experimental systems for studying the pathogenesis of typhoid and paratyphoid fever are limited. Therefore, STM infection of susceptible mice is commonly considered as model system for studying these diseases. The type III secretion system encoded by *Salmonella* pathogenicity island 2 (SPI2-T3SS) is a key factor for intracellular survival of *Salmonella*. Inside host cells, the pathogen resides within the *Salmonella*-containing vacuole (SCV) and induces tubular structures extending from the SCV, termed *Salmonella*-induced filaments (SIF). This study applies a set of single cell analyses approaches such as dual fluorescent protein reports, effector translocation, or correlative light and electron microscopy to investigate the fate and activities of intracellular STY and SPA. The SPI2-T3SS of STY and SPA is functional in translocation of effector proteins, SCV and SIF formation. However, only a low proportion of intracellular STY and SPA are actively deploying SPI2-T3SS and STY and SPA exhibited a rapid decline of protein biosynthesis upon experimental induction. A role of SPI2-T3SS for proliferation of STY and SPA in epithelial cells was observed, but not for survival or proliferation in phagocytic host cells. Our results indicate that reduced intracellular activities are factors of the stealth strategy of STY and SPA and facilitate systemic spread and persistence of the typhoidal *Salmonella*.

Introduction

Salmonella enterica is a versatile gastrointestinal pathogen with the ability to cause diseases ranging from acute, usually self-limiting gastroenteritis due to infections by non-typhoidal *Salmonella* (NTS) to severe systemic infections caused by typhoidal *Salmonella* (TS) serovars. Infections by *S. enterica* serovars such as Typhi (STY) and Paratyphi A (SPA) represent a continuing threat to human health. Particular in countries with low standards of hygiene, TS infections are endemic. The global burden of disease by TS infections is continuously high with about 27,000,000 infected people and 200,000 deaths annually worldwide, and the increased frequency of multidrug-resistant strains of TS, as well as coinfections cause problems for treatment of typhoid fever (Crump, Luby, & Mintz, 2004; Saleh et al., 2019).

While NTS infections are commonly associated with a strong inflammatory response leading to effective immune defense at the intestinal epithelium, TS infections lack this response and allow the pathogen to enter circulation and lymphatic system, and ultimately infect solid organs (reviewed in Dougan & Baker, 2014). The ability to survive phagocytosis and to persist and proliferate in infected host cells is considered a key virulence trait of *S. enterica* (Gal-Mor, 2019).

The restriction of STY and SPA to primate host organisms limits experimental approaches to study pathogenesis of typhoid and paratyphoid fever. Infection of susceptible mice by *S. enterica* sv. Typhimurium (STM) is commonly considered as model system for studying the diseases caused by highly human-adapted STY and SPA. Important virulence traits of *S. enterica* are also investigated on the cellular level using various cell culture systems for infection.

The type III secretion system encoded by *Salmonella* Pathogenicity Island 2 (SPI2-T3SS) is of central importance for systemic virulence of STM in a murine infection model, as well as for intracellular proliferation in cellular infection models with human or murine cells. Intracellular *Salmonella* within the SCV deploy the SPI2-T3SS to translocate into host cells a cocktail of

more than 30 effector proteins. These effector proteins manipulate various host cell functions such as vesicular transport, the actin and microtubule cytoskeleton, ubiquitination, apoptosis, releases of cytokines, antigen presentation by MHCII, and many more. Collectively, SPI2-T3SS effector proteins are required for intracellular survival and replication and the proliferation within host tissues. A remarkable difference between STM, STY and SPA is lack of a large number of SPI2-T3SS effector proteins in TS (reviewed in Jennings, Thurston, & Holden, 2017). This is due to absence of the virulence plasmid and bacteriophage genomes harboring effector genes, and the pseudogenization of effector genes. Thus, function of the SP2-T3SS and related phenotypes may be absent or altered in cells infected by STY or SPA. If findings on the role of SPI2-T3SS made in STM are also applicable to virulence of STY and SPA has not been investigated. A prior study reported that the SPI2-T3SS is not required for the intracellular survival and replication in the human macrophage cell line THP-1 which indicates that the SPI2 is not as important for STY as for STM (Forest, Ferraro, Sabbagh, & Daigle, 2010). Other studies reported requirement for SPI2-T3SS in release of typhoid toxin by cells infected by STY (Chang, Song, & Galan, 2016).

We set out to investigate the cellular microbiology of STY and SPA with focus on function of SPI2-T3SS and related phenotypes. To analyze the response of intracellular STM, STY or SPA to the host cell environment, we applied single cell-based approaches, such as fluorescence microscopy to follow translocation of effector protein, and correlative light and electron microscopy (CLEM) for ultrastructural analyses of the host cell endosomal system (Krieger et al., 2014), and potential manipulation by intracellular *S. enterica*. The fate of individual intracellular *S. enterica* is highly divergent (Birmingham, Smith, Bakowski, Yoshimori, & Brumell, 2006; Bumann, 2019; Helaine & Holden, 2013), thus we utilized various dual fluorescence reporters to determine the dynamic formation of distinct populations on single cell level.

Our analyses demonstrate that the SPI2-T3SS is functional in STY and SPA and mediate endosomal remodeling similar to STM. However, this manipulation of the host cell is only observed in a small number of host cells, and the frequency of STY and SPA showing intracellular activities is much lower compared to STM. The parsimonious deployment of virulence factors such as SPI2-T3SS can be considered as part of the stealth strategy of TS and may contribute to evade host immune responses.

Results

Genes encoding the SPI2-T3SS are induced in intracellular SPA and STY

To investigate the response of STY and SPA to the intracellular environment in various host cells, we analyzed if genes in SPI2 encoding the T3SS are expressed. For this, we used a fluorescent protein reporter with fusion of the promoter of *ssaG* in WT and Δ*ssrB* strains of STM, SPA or STY. Because *ssrB* is a local transcriptional regulator of genes encoding the SPI2-T3SS, we anticipated highly reduced activation of P_{ssaG}::sfGFP in Δ*ssrB* background (Hensel et al., 1998; Tomljenovic-Berube, Mulder, Whiteside, Brinkman, & Coombes, 2010). The functionality of the reporter was tested *in vitro* (**Fig. 1A**). In LB broth and minimal media with high phosphate concentration and neutral pH, referred to as PCN (25), pH 7.4, there was no induction of P_{ssaG}::sfGFP in STY and SPA, but slight induction in STM. In SPI2-inducing minimal media with a low phosphate concentration referred to as PCN (0.4), pH 5.8, P_{ssaG} induction was detected in WT strains of the three serovars, while no induction was detected in strains with deletion of *ssrB*. The function of reporter P_{ssaG}::sfGFP and the role of SsrB in controlling SPI2 promoters in intracellular *Salmonella* was further corroborated by microscopy of STM, STY or SPA-infected host cells. Representative micrographs for HeLa infection show the expression and absence of expression in WT or Δ*ssrB* background, respectively (**Fig. S 1**). We next determined P_{ssaG} induction by *Salmonella* in HeLa cells (**Fig. 1B**), U937 cells (**Fig. 1C**), RAW264.7 macrophages (**Fig. 1D**), or human primary macrophages (**Fig. 1E**) as host cells. In none of these host cells, the *ssrB* mutant strains showed P_{ssaG} induction, while induction was observed in STM, STY and SPA WT strains. In HeLa cells, the three serovars showed highest sfGFP intensities at 24 h p.i., with STM always showing higher sfGFP intensities than STY or SPA. In U937 cells, STM again showed the highest sfGFP levels at 8 h, 16 h and 24 h p.i. While the intracellular population of STM and SPA showed rather uniform induction, a heterogeneous response was observed for intracellular STY, with single cells showed various

levels ranging from very low to high sfGFP intensities. At 24 h p.i., the distribution of the STY population changed, and sfGFP intensity increased. In the murine macrophage-like cell line RAW264.7 at 16 h p.i., the sfGFP intensities were similar for STM, STY and SPA. After activation of RAW264.7 by interferon γ (IFN-γ) STY only produced very low sfGFP fluorescence, SPA showed higher intensities, and highest signal intensities were observed for STM (**Fig. 1D**). In human primary macrophages, only a part of the population of SPA and STM WT showed higher sfGFP levels than the Δ*ssrB* strains (**Fig. 1E**).

As a complementary approach, we analyzed U937 cells infected by STM, STY or SPA for induction of the P_{ssaG}::sfGFP reporter (**Fig. 2**). While the majority of intracellular STM showed induction of P_{ssaG}::sfGFP at 8 h p.i., a lower frequency was observed for STY and SPA under these conditions. Some U937 cells only contained P_{ssaG}-negative STY or SPA, while a larger number of host cells harbored mixtures of P_{ssaG}-positive as well as P_{ssaG}-negative bacteria.

The SPI2-encoded type III secretion system is functional in STY and SPA

Mutant strains of STM deficient in SPI2-T3SS function are highly attenuated in murine models of systemic disease, as well as in intracellular survival and proliferation in various types of murine and human host cells (Hensel et al., 1995; Hensel et al., 1998; Ochman, Soncini, Solomon, & Groisman, 1996). Genes encoding the SPI2-T3SS are present in STY and SPA and are not affected by pseudogenization. However, the functionality of SPI2-T3SS in STY and SPA has not been demonstrated experimentally.

We investigated the translocation of SPI2-T3SS effector proteins by intracellular STY or SPA (**Fig. 3**). For this, mutant strains deficient in the core components of SPI2-T3SS were generated by Red-mediated mutagenesis. Because antisera against effector proteins of the SPI2-T3SS are limited in availability and quality, we introduced low copy number plasmids for the expression of alleles of representative effector proteins SseF, SseJ, PipB2, and SseL tagged with HA or M45 epitope tags. Prior work reported the translocation of these tagged effector proteins by STM, and their association with late endosomal/lysosomal host cell membranes (Coombes et

al., 2007; Hansen-Wester, Stecher, & Hensel, 2002; Knodler et al., 2003; Kuhle & Hensel, 2002).

We observed that effector proteins were translocated into HeLa cells infected by STY or SPA WT (**Fig. 3AB**). No signals for translocated effector proteins were detected after infection with SPI2-T3SS-deficient strains, as shown for representative STY Δ*ssaK* [*sseF*::M45] (**Fig. 3C**). The signal intensities of effectors translocated by STY varied, with stronger accumulation of SseF and SseL, while signals for SseJ were rather weak. After translocation by SPA, signals of similar high intensities were detected. The amounts of effector proteins detected in STY- or SPA-infected host cells were lower than for STM-infected host cells (data not shown). Also, the frequency of STY- or SPA-infected host cells that were positive of effector signals was lower.

We conclude that the SPI2-T3SS is functional in translocation of effector proteins by intracellular STY and SPA. However, a lower proportion of intracellular STY and SPA actively translocate SPI2-T3SS effector proteins. Translocation of SseJ is possible in STY and SPA, although *sseJ* is a pseudogene in these serovars (Jennings *et al*., 2017).

SPA and STY inhabit an SCV in infected host cells and remodel the endosomal system

Several prior analyses have demonstrated that STM inhabits an individual SCV (Krieger et al., 2014; Rajashekar, Liebl, Seitz, & Hensel, 2008). A representative marker for this compartment is LAMP1, a member of the family of lysosomal glycoproteins that are membrane integral in late endosomal and lysosomal membranes. Previous work described that each intracellular bacterium is complete enclosed by LAMP1-positive membranes, resulting in individual pathogen-containing compartments (Rajashekar, Liebl, Chikkaballi, Liss, & Hensel, 2014). We investigated the formation of SCV in HeLa LAMP1-GFP (**Fig. 4**) or RAW264.7 LAMP1-GFP cells (**Fig. S 2**) infected with STM, STY, or SPA.

The massive reorganization of the endosomal system was observed in mammalian host cells infected by STM. One consequence of this reorganization is the formation of extensive tubular

vesicles. *Salmonella*-induced filaments (SIF) are tubular vesicles characterized by the presence of late endosomal/lysosomal membrane markers. We investigated the formation of SIF in SPA- or STY-infected host cells. Endosomal remodeling depends on function of the SPI2-T3SS, and effector protein SifA is essential for SIF formation and integrity of the SCV (Beuzon et al., 2000; Stein, Leung, Zwick, Garcia-del Portillo, & Finlay, 1996). Infected cells were analysed for formation of SIF and we compared intracellular phenotypes of WT and Δ*sifA* strains of the various serovars. In infected HeLa or RAW cells, we observed formation of LAMP1-GFP-positive membrane compartments that completely enclosed individual bacteria (**Fig. 4A**). The formation of SIF was observed in host cells infected with STM, STY or SPA WT strains, while STY Δ*sifA* (**Fig. 4A**) or SPA Δ*sifA* (data not shown) strains did not induce SIF. In RAW264.7 macrophages, LAMP1-positive compartments were observed after phagocytosis of STM, STY, or SPA WT or SPI-T3SS-deficient strains (**Fig. S 2**). Since imaging was performed using fixed cells, SIF induction in macrophages was not assessed.

The frequency of SIF-positive cells infected with WT or Δ*sifA* strains was quantified in HeLa cells at 16 h and 24 h p.i. (**Fig. 4B**). In line with prior observations, STM WT induced SIF in the majority of infected cells, while tubular endosomes were almost absent after infection by the STM Δ*sifA* strain (1-2% positive cells). SIF formation in cells infected by STY or SPA was much less frequent and only 5% to 10% were scored positive. Cells infected with STY or SPA Δ*sifA* strains very rarely showed tubular endosomal compartments.

We further characterized the SCV using canonical markers of the endocytic pathway. The small GTPases Rab7A and Arl8A were transiently transfected in HeLa cells. To mark late endosomes and lysosomes in HeLa cells, we used fluid phase marker Dextran-Alexa647. The association of Rab7A and Arl8A with SCV and SIF was frequently observed in cells infected with STY or SPA (**Fig. S 3**).

We conclude that SPI2-T3SS and effector SifA can mediate endosomal remodeling by STY and SPA. However, the frequency of this manipulation of host cell functions by STY and SPA

is highly reduced compared to STM. A role of SifA in maintaining the integrity of SCV containing STY or SPA cannot be deduced from our experimental data. The molecular composition of endosomal compartments modified by STM, STY or SPA is similar.

SPA and STY induce the formation of double-membrane SIF

We have recently unraveled the unique architecture of SIF induced by STM in epithelial cells and macrophages (Krieger et al., 2014). In particular, tubular compartments were delimited by vesicular single membranes, and at later time points after infection, SIF composed of double membranes were frequently observed. We analyzed if SIF induced by intracellular STY and SPA are comparable in architecture, or distinct to SIF observed in STM-infected cells. We performed CLEM analyses in order to reveal the ultrastructural features of SIF networks identified by light microscopy (**Fig. 5**). Although the frequency of STY- or SPA-infected cells with SIF was low, light microscopy allowed identification of these events for subsequent TEM analyses. As for STM, SCV harboring STY or SPA were continuous and in close contact to the bacterial envelope. In cells with an extensive SIF network, characteristic double-membrane SIF were observed in HeLa cells infected by STM, as well as by SPA, or STY (**Fig. 5**, **Fig. S 4**, **Fig. S 5**, **Fig. S 6**). SIF extending into the cell periphery were connected to the SCV. The morphological characteristics of the tubular compartments appeared comparable for the three serovars, as well as the diameter of app. 160 nm.

We conclude that STY and SPA can induce tubular endosomal networks comparable to those characterized in STM-infected cells.

SCV integrity and cytosolic access of intracellular STY and SPA

Maintenance of the integrity of the SCV is important for virulence of STM, and mutant strains deficient in SPI2-T3SS effector protein SifA are more frequently released into the cytosol of host cells. Host cells respond to cytosolic STM with xenophagic clearance, or induction of pyroptotic cell death (Birmingham et al., 2006). In epithelial cells, cytosolic hyper-replication

of STM can lead to killing of host cells, or triggers expulsion of infected cells from polarized epithelial layers (Knodler et al., 2010). In contrast to STM, the importance of SCV integrity and potential contribution of SifA is not known for TS.

We recently used a dual fluorescence reporter plasmid for analyses of exposure of intracellular bacteria to host cell cytosol as result of impaired SCV integrity (Röder & Hensel, 2020). The sensor is based on the promoter of *uhpT*, a transporter for glucose-6-phosphate (G6P). As G6P is present in the cytosol of mammalian host cells, but is rapidly metabolized in bacterial cells, specific induction of this reporter occurs in STM that are in contact with host cell cytosol.

We tested the dual fluorescence cytosolic sensor in SPA and STY using *in vitro* growth conditions with various amounts of G6P (**Fig. 6A**).While STY showed a G6P concentration-dependent increase in sfGFP fluorescence similar to prior observations of STM (Röder & Hensel, 2020), no induction was observed for SPA. Analyses of the genome sequence of SPA indicated that the sensor-regulator system encoded by *uhpABC* is defective by pseudogene formation (Holt et al., 2009), and activation of P_{uhpT} is not possible. Thus, the P_{uhpT}-based cytosolic sensor was not applied to analyses of SPA.

We compared cytosolic exposure of STM and STY in HeLa cells (**Fig. 6B**), or U937 macrophages (**Fig. 6C**). A rather large cytosolic-induced population was observed for STM, which increased over time. As a STM Δ*sifA* strain was reported to be deficient in maintaining the integrity of the SCV, we also determined cytosolic release of a STY Δ*sifA* strain. In HeLa cells infected with STM WT two populations were apparent, a sfGFP-positive population indicating cytosolic exposure, and one population without sfGFP fluorescence indicating segregation from host cell cytosol. At 16 h or 24 h p.i., STM Δ*sifA* was homogenously sfGFP-positive. For STY WT, only a small population was sfGFP-induced and this population decreases over time p.i. Only very low numbers of sfGFP-positive, cytosol-exposed STY Δ*sifA* were detected at any timepoint. In U937 cells, a sfGFP-positive population was only detected for STM Δ*sifA* at 16 or 24 h p.i. Cytosolic presence of *Salmonella* in phagocytes is known to

trigger pyroptosis (Bergsbaken, Fink, & Cookson, 2009), and this response was also induced by STM Δ*sifA*. However, since FC was used to analyze the same number of infected cells for the various conditions, this likely revealed the subpopulation of pre-pyroptotic macrophages harboring cytosolic-induced STM Δ*sifA*. STM WT and STY WT and Δ*sifA* strain did not show sfGFP fluorescence signals, indicating very low numbers of intracellular *Salmonella* exposed to host cell cytosol.

The intracellular proliferation of SPI2-T3SS-deficient STY is reduced in HeLa cells

Prior work corroborated that function of SPI2-T3SS is required for intracellular proliferation of STM in various cell lines and in tissue of infected hosts (Shea, Hensel, Gleeson, & Holden, 1996). The role of SPI2-T3SS for intracellular proliferation of TS is still open. This lack of information and the functionally of the SPI2-T3SS demonstrated here prompted us to test for STM, STY and SPA intracellular proliferation as function of SPI2-T3SS by gentamicin protection assays (**Fig. 7**). Intracellular proliferation of SPI2-T3SS-deficient STM Δ*ssaV* in HeLa was reduced about 10-fold. SPI2-T3SS-deficient STY Δ*ssaR* was similar with about 8-fold attenuation compared to WT. While SPI2-T3SS-deficient STM were highly and moderately attenuated in proliferation in RAW264.7 and U937 macrophages, respectively, no attenuation was observed for STY *ssaR*.

The data shown in **Fig. 1** and **Fig. 4** indicate that only a small fraction of intracellular STY or SPA deploys the SPI2-T3SS. Thus, the intracellular proliferation of STY may be low overall, and the deficient in proliferation of a SPI2-T3SS-deficient strain may be masked by a large number of intracellular STY that survive but fail to proliferate. To address intracellular proliferation on the levels of single host cells, we deployed FC and determined mCherry-mediated fluorescence as proxy for bacterial load. We recently compared properties of various FP and identified fast-maturing, constitutively expressed mCherry as reliable indicator for proliferation of intracellular bacteria (Schulte, Olschewski, & Hensel, 2020).

Analyses of single host cells (**Fig. 8**, **Fig. S 7**) confirmed the SPI2-T3SS-dependent intracellular proliferation of STM in HeLa, RAW264.7 and U937, and of STY in HeLa. The X-means for RAW264.7 or U937 harboring STY also increased from 1 h p.i. to 24 h p.i. This increase was rather small and independent from function of the SPI2-T3SS. Interestingly, STM also showed SPI2-T3SS-independent increase of bacterial mCherry fluorescence in HeLa, RAW264.7, and U937 cells, but the increase was always reduced compared to proliferation of STM WT.

Taken together, these results support a role of SPI2-T3SS in intracellular proliferation of STY in HeLa cells, and redundancy of SPI2-T3SS function for proliferation in the phagocytic cell lines investigated.

Biosynthetic capability of intracellular STM, SPA and STY

Finally, we set out to determine the proportion of intracellular STM, SPA or STY that remain capable in protein biosynthesis upon application of an external stimulus. We anticipated that dead bacteria, and those that have entered a persister state are highly reduced in protein biosynthesis and unable to respond to an external stimulus. As experimental system, we introduced in STM, STY and SPA a dual fluorescence plasmid for constitutive expression of DsRed, and expression of sfGFP under control of the promoter of *tetA*. We recently demonstrated that P_{tetA} can be efficiently activated in intracellular *Salmonella* by external addition of the inducer anhydrotetracycline (AHT) (Schulte et al., 2019). Under culture conditions in medium, sfGFP synthesis was induced by addition of AHT in STM, SPA or STY to comparable levels (**Fig. 9A**). After infection of various host cell types by STM, SPA or STY, inducer AHT was added to infected cells 1.5 h prior to the end of the infection period and lysis of host cells (**Fig. 9B**). In HeLa cells 8 h p.i., around 80% of the bacteria showed induction, and the intensities for STY cells were higher than for STM and SPA (**Fig. 9C**). The proportion of induced STM remained high at 16 h and 24 h p.i., while the percentage of AHT-induced STY and SPA declined at 16 h and 24 h p.i., as well as sfGFP intensities of induced *Salmonella*.

In human U937 macrophages (**Fig. 9D**), a similar percentage of AHT-inducible bacteria was determined 8 h p.i. for all serovars. At later time points p.i., the amounts of AHT-inducible SPA and STY dropped, while STM remained at more than 85% AHT-inducible bacteria at all time points.

In murine RAW264.7 macrophages (**Fig. 9E**), we observed a high percentage of AHT-inducible STM, SPA, and STY at the early time point of 3 h p.i., however, the level of sfGFP fluorescence was lower in the induced SPA population compared to induced STM and STY. A further decrease in sfGFP expression was observed for SPA at 8 h p.i., while the percentage of induced STM and STY increased to more than 92%. At 24 h p.i. STM showed a large population of AHT-inducible cells (64%), while the population of AHT-inducible STY was decreased in size, and induced STY showed lower sfGFP intensities. For SPA, an almost complete shift to the non-inducible population was observed.

The analyzed serovars are rather distinct in their ability to respond to intracellular environments. STM appeared most robust and biosynthetic active populations of similar size were detected in all host cell types and any time point. STY showed highest percentage of biosynthetic active bacteria at early time points in all cell lines analyzed, and the proportion of AHT-inducible cells decreased in all host cell types at 16 and 24 h p.i. The level of sfGFP expression of proportion of AHT-inducible SPA was already reduced at early time points and further decreased over time, indicating a continuous loss of biosynthetic capacity over time. The effect was most pronounced in RAW264.7 cells. We conclude that STY and SPA have a lower capacity than STM to maintain a biosynthetic active state over prolonged presence in host cells.

Discussion

Our study investigated the intracellular lifestyle of STY and SPA as clinically most relevant serovars of TS. We demonstrated that SPI2-T3SS is functional in translocating effector proteins that induce endosomal remodeling, and formation and maintenance of SCV. The SPI2-T3SS-dependent remodeling of the endosomal system by STY and SPA was reminiscent of the phenotypes observed in STM-infected cells. By this, we provide formal proof of the function of the SPI2-T3SS in human-adapted TS serovars. As major difference in intracellular phenotypes of SPA and STY compared to STM, we observed the delayed activation and overall lower frequency of intracellular *Salmonella* showing activity of SPI2-T3SS and related phenotypes. Furthermore, the population of intracellular STY exhibits larger heterogeneity. In the following these aspects are discussed in more detail.

Low intracellular activity of TS

Compared to STM, intracellular STY and SPA formed smaller populations of bacteria with SPI2-T3SS function and more general, biosynthetic activity in response to artificial induction. SPI2-T3SS function mediated proliferation in HeLa but not in the more restrictive environment of macrophages. These observations indicate that STY and SPA are either more efficiently killed by host cells, or more frequently develop persister state. Persister bacteria are key contributors to persistent as well as recurring infections (Lewis, 2010), and both phenomena are characteristic to infectious diseases caused by TS (Gal-Mor, 2019). Future studies have to reveal the role of persister formation of intracellular STY and SPA and the contribution of persister bacteria to pathogenesis of TS infections.

Role of the SPI2-T3SS in TS

We previously demonstrated that SP2-T3SS-mediated SIF formation augments nutritional supply of STM in the SCV, and also leads to reduction of antimicrobial factors acting on bacteria in the SCV (Liss et al., 2017; Noster et al., 2019). Since SIF formation is less frequent

in host cells infected by STY or SPA compared to STM, this may indicate a restricted nutritional supply, leading to limited intracellular proliferation. As STY and SPA are auxotrophic for cysteine and tryptophan (McClelland et al., 2004) the demand for external supply with amino acids is higher than for prototrophic STM. Furthermore, exposure to effectors of host cell defense mechanisms may be increased for STY or SPA in SCV without SIF connection. Further single cell analyses can address this potential correlation between SIF formation and proliferation for intracellular TS.

Our work confirms prior reports that SPI2-T3SS is not required for net survival and proliferation of STY in infection models with human macrophages (Forest et al., 2010). Our observation that only a small percentage of bacteria synthesize SPI2-T3SS and deploy its function would also allow alternative explanations. In ensemble-based analyses such as the gentamicin protection assay, ongoing proliferation in a small number of infected host cells may by masked by the majority of infected cells that kill the pathogen or restrict its proliferation. Even if the number of permissive infected cells is low, these may play an important role for progression of a systemic infection (Brown et al., 2006). The application of single cell FC analyses will allow future in-depth analyses of the fate of TS in distinct subpopulations of host cells.

Role of SPI2-T3SS effector proteins in TS

The SPI2-T3SS in STM translocates a complex set of more than 30 effector proteins into infected host cells. These effector proteins form subsets that act on the endosomal system, affect innate immune signaling, formation of adaptive immunity, interfere with ubiquitination, or have functions still unknown (Jennings et al., 2017). The repertoire of effector proteins in STY and SPA is severely restricted, with intact genes only for 11 or 8 effectors proteins in STY and SPA, respectively (Jennings et al., 2017). This observation may reflect the adaptation to a narrow host range accompanied by loss of redundant effectors. Of note, the subset of effector proteins involved in endosomal remodeling (SseF, SseG, SifA, PipB2, SteA) is present. We showed that

SifA is required for induction of SIF formation in STY and SPA similar to STM. However, our analyses did not support a contribution of SIF in maintaining the SCV integrity in cells infected by STY. Among other sequence variations, the altered sequence of the C-terminal membrane anchoring hexapeptide (Boucrot, Beuzon, Holden, Gorvel, & Meresse, 2003) may affect function of SifA in STY.

Also present in STM, STY and SPA is SteD, an effector protein modulating adaptive immunity (Bayer-Santos et al., 2016). The activation of CD4+ T cells is very important for the elimination of *Salmonella* in mice and human. In STM, SteD stimulates the ubiquitination of MHCII, leading to its degradation and therefor prevention of antigen presentation by MHCII (Bayer-Santos et al., 2016). SteD is present in STY and SPA, but shows subtile differences in amino acid sequence. Thus, it is not certain whether SteD exhibits the same function in STY or SPA as in STM. Because interference with host adaptive immunity is of central importance of persistent infections as caused by TS, the function of SteD in STY and SPA deserves further investigation.

It was reported that effector protein SteE of STM directs macrophage polarization towards an anti-inflammatory M2 state (Stapels et al., 2018). However, STY and SPA lack SteE and are unlikely to manipulate the activation state of macrophages by this mechanism. Uptake by macrophages may be fatal for individual STY or SPA during infection, and phagocytic cells with other properties, such as dendritic cells, could form important vehicles of systemic distribution of TS. Again, host specificity and low numbers of STY- or SPA-infected cells in human blood are obstacles to more detailed analyses.

Additional effector proteins that are specific to STY and SPA may be present and mediate serovar-specific properties. One example is StoD, an E3/E4 ubiquitin ligase that is translocated by the SPI1-T3SS (McDowell et al., 2019). A systematic screen by bioinformatics tools and experimental validation may identify TS-specific effector proteins of SPI2-T3SS.

Need of suitable infection models for TS

We observed distinct intracellular phenotypes in the various cell lines and primary cells used in this study. However, the specific virulence properties of TS and the contribution of SPI2-T3SS require analyses in improved infection models. Of specific interest will be organoids of human origin that are capable to simulate tissues that are infected by STY or SPA. In the human body, STY persistently colonizes gallbladder and bone marrow. *Salmonella* is resistant to high concentrations of bile and bile also has an influence on the invasion of epithelial cells by *Salmonella* (Prouty, Schwesinger, & Gunn, 2002). Bile induces persister cell formation of STY and an associated tolerance to antibiotics (Walawalkar, Vaidya, & Nayak, 2016). It is also known that STY forms biofilm in the gallbladder and on gallstones. This could lead to constant inflammation of gallbladder tissue, and during persistent infection to development of gallbladder cancer (Di Domenico, Cavallo, Pontone, Toma, & Ensoli, 2017). The formation of biofilm enables STY to adapt a carrier state in the host, which occurs in about 3 – 5% of the infected people (Prouty et al., 2002). For example, a recently organoid model to human gallbladder epithelium may provide new options to study TS in a setting of a persistent infection (Sepe et al., 2020). If SPI2-T3SS effector functions beyond intracellular survival and proliferation should be analyzed, even more complex experimental systems with human immune cells are required. As alternative, a humanized mouse model based on transplantation of human immune cells may be considered (Karlinsey et al., 2019). A genome-wide screen for genes required for survival in STY in humanized mice did not reveal contributions of SPI2-T3SS or effector protein. Since the initial screen was performed using an infection period of 24 h, identification of STY factors affecting formation of adaptive immune responses were not identified. Future analyses in the humanized mouse model under conditions allowing persistent infection will be of interest, but the high demands of the complex model may compromise more frequent applications.

Concluding remarks

This study demonstrated that the functionality of SPI2-T3SS in STY and SPA, and future studies with improved infection models have to reveal the contribution of this virulence factor to pathogenesis of infectious diseases by TS. We applied a set of single cell approaches to study the intracellular adaptation strategies of STM as NTS serovar in comparison to TS serovars STY and SPA. These analytic tools enabled a detailed view on the specific intracellular activities of NTS and TS, and will enable future in-depth characterization of bacterial heterogeneity and adaptation strategies.

Acknowledgements

This work was supported by BMBF grant within the Infect-ERA consortium SalHostTrop. We thank Dr. Ohad Gal-Mor for providing STY and SPA strains, and the members of the SalHostTrop consortium for fruitful discussions.

Materials and Methods

Bacterial strains and culture conditions

For this study *Salmonella enterica* serovar Typhimurium (STM) NCTC12023, *S. enterica* serovar Typhi (STY), and *S. enterica* serovar Paratyphi A (SPA) were used as wild-type (WT) strains. All mutant strains are isogenic to the respective WT and Table 1 shows characteristics of strains used in this study. STM, STY and SPA strains were routinely grown on Luria-Bertani broth (LB) agar or in LB broth containing 50 µg x ml^{-1} carbenicillin for maintenance of plasmids at 37 °C using a roller drum. As synthetic media, PCN (Phosphate, Carbon, Nitrogen) was used as described before (Löber, Jäckel, Kaiser, & Hensel, 2006) with the indicated pH concentrations of inorganic phosphate. For culture of STY and SPA, PCN media were supplemented with 20 µg x ml^{-1} of each cysteine and tryptophan.

Generation of bacterial strains

Mutant strains harboring deletions in various virulence genes were generated by λ Red recombineering for insertion of the kanamycin resistance cassette amplified from template plasmid pKD13 basically as described before (Chakravortty, Hansen-Wester, & Hensel, 2002; Datsenko & Wanner, 2000) using oligonucleotides listed in Table S 2. The proper insertion was confirmed by colony PCR. If required, the *aph* cassette was removed by introduction of pE-FLP and FLP-mediated recombination. Plasmids used in this study are listed in Table 2 and were introduced into various WT and mutant strains by electroporation.

Host cell culture and infection

The murine macrophage cell line RAW264.7 (American Type Culture Collection, ATCC no. TIB-71) was cultured in high-glucose (4.5 g x ml^{-1}) Dulbecco's modified Eagle's medium (DMEM) containing 4 mM stable glutamine (Merck) and supplemented with 6% inactivated fetal calf serum (iFCS, Sigma). The human macrophage-like cell line U937 (ATCC no. CRL-1593.2) was cultured in RPMI-1640 medium (Merck) supplemented with 10% iFCS. Human

primary macrophages isolated from buffy coat were cultured in RPMI-1640 medium supplemented with 20% iFCS. The non-polarized epithelial cell line HeLa (ATCC no. CCL-2) was cultured in high-glucose DMEM containing 4 mM stable glutamine, sodium pyruvate and supplemented with 10% iFCS. Stably transfected HeLa cell lines expressing LAMP1-GFP were cultured under the same conditions. All cells were cultured at 37 °C in an atmosphere containing 5% CO_2 and absolute humidity.

Gentamicin protection assay

The assay was performed as described before (Kuhle & Hensel, 2002). Briefly, RAW264.7 cells were seeded 24 or 48 h prior infection in a surface-treated 24 well plate (TPP) to reach confluency (~4 x 10^5 cells per well) on the day of infection. U937 cells were seeded 72 h prior infection in surface-treated 24 well plates (TPP) to reach confluency (~4 x 10^5 cells per well) on the day of infection and were treated with 50 ng x μl^{-1} PMA for differentiation and cell attachment. HeLa cells were seeded 48 h prior infection in surface-treated 24 well plates (TPP) to reach confluency (~2 x 10^5 cells per well) on the day of infection. For infection of RAW264.7 and U937 cells, bacteria were grown overnight (~ 20 h) aerobically in LB medium. For infection of HeLa cells, fresh LB medium was inoculated 1:31 with overnight cultures of STM and incubated for 2.5 h with agitation. For subculture of STY and SPA, 10 ml fresh LB medium was inoculated 1:100 with aerobic over day cultures and grown static under microaerophilic conditions for 16 h (Elhadad, Desai, Rahav, McClelland, & Gal-Mor, 2015). Then the bacteria were adjusted to an OD_{600} of 0.2 in PBS and further diluted in DMEM (RAW and HeLa cells) or RPMI medium (U937 cells) for infection of cells at a MOI of 1. Bacteria were centrifuged onto the cells for 5 min at 500 x g, and the infection was allowed to proceed for 25 min. After three washing steps with PBS, medium containing 100 µg x ml^{-1} gentamicin was added for 1 h to kill extracellular bacteria. Afterwards the cells were incubated with medium containing 10 µg x ml^{-1} gentamicin for the ongoing experiment. Cells were washed three times with PBS and lysed using 0.1% Triton X-100 at 2 and 24 h post infection (p.i.). Colony forming units (CFU)

were determined by plating serial dilutions of lysates and inoculum on Mueller-Hinton II agar and incubated overnight at 37 °C. The percentage of phagocytosed bacteria as well as the replication rate was calculated.

Infection experiments for microscopy

HeLa cells stably transfected and expressing LAMP1-GFP were seeded in 24 well plates (TPP) on coverslips. The cells were grown to 80% confluency (~ 1.8 x 10^5) on the day of infection. The cells were infected with STM, STY and SPA strains as described above with aerobic 2.5 h (for STM) and microaerobic, static 16 h (for STY, SPA) bacterial subcultures. For detection SPI2-T3SS effector protein translocation, MOI of 75 was used for infection and cells were analyzed 9 h p.i. For visualization of bacteria harboring reporter plasmids, MOI 50 was used for STM and SPA, and MOI 75 was used for STY. Afterwards the cells were washed three times with PBS and fixed with 3% paraformaldehyde (PFA) in PBS.

Transfection

HeLa cells were cultured in 8-well dishes (ibidi) for one day. One µg of plasmid DNA of various transfection vectors was diluted in 25 µl DMEM without iFCS and mixed with 1 µl FUGENE reagent (ratio of 1:2 for DNA to FUGENE). The transfection mix was incubated for 10 min at room temperature (RT) and added to the cells in DMEM with 10% iFCS for at least 18 h. Before infection, the cells were treated with fresh medium.

Pulse-chase with fluid phase markers

The fluid phase marker AlexaFluor 647-conjugated dextran (dextran-A647), molecular weight 10,000 (Molecular Probes) was used for tracing the endocytic pathway. HeLa cells were incubated with 100 µg x ml^{-1} dextran-A647 1 h p.i. until fixation of the cells. Subsequently, cells were washed and prepared for microscopy.

Immuno-staining and fluorescence microscopy

Cells fixed with 3% PFA were washed three times with PBS and incubated in blocking solution (2% goat serum, 2% BSA and 0.1% saponin in PBS) for 30 min. Next, cells were stained for 1 h at RT with primary antibodies against *Salmonella* O-Ag of STM, STY and SPA (1:500), anti-HA (1:500) or anti-M45 (1:10). Accordingly, secondary antibodies were selected and samples were incubated for 1 h. Antisera and antibodies used in this study are listed in Table S 1. Coverslips were mounted with Fluoroprep (Biomerieux) and sealed with Entellan (Merck). The microscopy was performed with the confocal laser-scanning microscope Leica SP5 using the 100x objective (HCX PL APO CS 100 x, NA 1.4-0.7) and the polychroic mirror TD 488/543/633 for the three channels GFP, TMR/Alexa568, Cy5 (Leica, Wetzlar, Germany). For image processing, the LAS-AF software (Leica, Wetzlar, Germany) was used.

Flow cytometry analyses

Cells were seeded in 12-well plates (TPP) 48 h (HeLa and RAW264.7), or 72 h (U937) prior infection to reach confluency on the day of infection (HeLa cells: 4 x 10^5 cells/well, RAW264.7: 8 x 10^5 cells/well, U937: 7 x 10^5 cells/well). U937 cells were treated with 50 ng x μl^{-1} PMA. RAW264.7, HeLa or U937 cells were infected with STM, STY and SPA WT or Δ*ssrB* and Δ*sifA* strains at MOI of 30 as described before. The bacterial strains harbored plasmids constitutively expressed RFP (p3776, p4928) or DsRed (p4889), and expressed sfGFP after activation of respective promotors. To determine metabolic activity, cells infected with *Salmonella* harboring plasmid p4928 were induced 2 h before fixation by addition of AHT to 50 ng x ml^{-1}. At 8, 16, or 24 h p.i., cells were washed with PBS, detached from the culture plates, lysed with 0.1% Triton X-100, fixed with 3% PFA and analyzed by flow cytometry using an Attune NxT cytometer (Life Technologies, Thermo Fischer). At least 10,000 RFP- or DsRed-positive cells were measured and the cells expressing red and green fluorescence were analyzed.

Flow cytometry analyses of whole cells

Cells were seeded in 6 well plates (TPP) 48 h (HeLa and RAW264.7), or 72 h (U937) prior infection to reach confluency on the day of infection (HeLa cells: 8 x 10^5 cells/well, RAW264.7: 1.6 x 10^6 cells/well, U937: 1.4 x 10^6 cells/well). U937 cells were treated with 50 ng x μl^{-1} PMA. RAW264.7, HeLa or U937 cells were infected with STM, STY and SPA WT or SPI2-T3SS-deficient strains (Δ*ssaV,* Δ*ssaK,* or Δ*ssaR*) at MOI 10 as described before. The bacterial strains harbored plasmids constitutively expressing mCherry. At 1 h and 24 h p.i., cells were washed with PBS, detached form the culture plates, fixed with 3% PFA and analyzed by flow cytometry using an Attune NxT cytometer. At least 10,000 mCherry-positive cells were measured and intensities of mCherry fluorescence signals per host cell were quantified.

References

Bayer-Santos, E., Durkin, C. H., Rigano, L. A., Kupz, A., Alix, E., Cerny, O., . . . Holden, D. W. (2016). The *Salmonella* effector SteD mediates MARCH8-dependent ubiquitination of MHC II molecules and inhibits T cell activation. *Cell Host Microbe, 20*(5), 584-595. doi:10.1016/j.chom.2016.10.007

Bender, J. K., Wille, T., Blank, K., Lange, A., & Gerlach, R. G. (2013). LPS structure and PhoQ activity are important for *Salmonella* Typhimurium virulence in the *Galleria mellonella* infection model [corrected]. *PLoS One, 8*(8), e73287. doi:10.1371/journal.pone.0073287

Bergsbaken, T., Fink, S. L., & Cookson, B. T. (2009). Pyroptosis: host cell death and inflammation. *Nat. Rev. Microbiol., 7*(2), 99-109. doi:nrmicro2070 [pii] 10.1038/nrmicro2070

Beuzon, C. R., Meresse, S., Unsworth, K. E., Ruiz-Albert, J., Garvis, S., Waterman, S. R., . . . Holden, D. W. (2000). *Salmonella* maintains the integrity of its intracellular vacuole through the action of SifA. *EMBO J, 19*(13), 3235-3249. doi:10.1093/emboj/19.13.3235

Birmingham, C. L., Smith, A. C., Bakowski, M. A., Yoshimori, T., & Brumell, J. H. (2006). Autophagy controls *Salmonella* infection in response to damage to the *Salmonella*-containing vacuole. *J Biol Chem, 281*(16), 11374-11383. doi:10.1074/jbc.M509157200

Boucrot, E., Beuzon, C. R., Holden, D. W., Gorvel, J. P., & Meresse, S. (2003). *Salmonella typhimurium* SifA effector protein requires its membrane-anchoring C-terminal hexapeptide for its biological function. *J Biol Chem, 278*(16), 14196-14202. doi:10.1074/jbc.M207901200

Brown, S. P., Cornell, S. J., Sheppard, M., Grant, A. J., Maskell, D. J., Grenfell, B. T., & Mastroeni, P. (2006). Intracellular demography and the dynamics of *Salmonella enterica* infections. *PLoS Biol, 4*(11), e349. doi:10.1371/journal.pbio.0040349

Bumann, D. (2019). *Salmonella* single-cell metabolism and stress responses in complex host tissues. *Microbiol Spectr, 7*(2). doi:10.1128/microbiolspec.BAI-0009-2019

Chakravortty, D., Hansen-Wester, I., & Hensel, M. (2002). *Salmonella* pathogenicity island 2 mediates protection of intracellular *Salmonella* from reactive nitrogen intermediates. *J Exp Med, 195*(9), 1155-1166. doi:10.1084/jem.20011547

Chang, S. J., Song, J., & Galan, J. E. (2016). Receptor-mediated sorting of typhoid toxin during its export from *Salmonella* Typhi-infected cells. *Cell Host Microbe, 20*(5), 682-689. doi:10.1016/j.chom.2016.10.005

Coombes, B. K., Lowden, M. J., Bishop, J. L., Wickham, M. E., Brown, N. F., Duong, N., . . . Finlay, B. B. (2007). SseL is a *Salmonella*-specific translocated effector integrated into the SsrB-controlled *Salmonella* pathogenicity island 2 type III secretion system. *Infect Immun, 75*(2), 574-580. doi:10.1128/IAI.00985-06

Crump, J. A., Luby, S. P., & Mintz, E. D. (2004). The global burden of typhoid fever. *Bull World Health Organ, 82*(5), 346-353. Retrieved from https://www.ncbi.nlm.nih.gov/pubmed/15298225

Datsenko, K. A., & Wanner, B. L. (2000). One-step inactivation of chromosomal genes in *Escherichia coli* K-12 using PCR products. *Proc. Natl. Acad. Sci. U S A, 97*(12), 6640-6645. Retrieved from 10829079

Di Domenico, E. G., Cavallo, I., Pontone, M., Toma, L., & Ensoli, F. (2017). Biofilm producing *Salmonella* Typhi: chronic colonization and development of gallbladder cancer. *Int J Mol Sci, 18*(9). doi:10.3390/ijms18091887

603 Dougan, G., & Baker, S. (2014). *Salmonella enterica* serovar Typhi and the pathogenesis of
604 typhoid fever. *Annu Rev Microbiol, 68*, 317-336. doi:10.1146/annurev-micro-091313-
605 103739
606 Drecktrah, D., Levine-Wilkinson, S., Dam, T., Winfree, S., Knodler, L. A., Schroer, T. A., &
607 Steele-Mortimer, O. (2008). Dynamic behavior of *Salmonella*-induced membrane
608 tubules in epithelial cells. *Traffic, 9*(12), 2117-2129. doi:TRA830 [pii]
609 10.1111/j.1600-0854.2008.00830.x
610 Elhadad, D., Desai, P., Rahav, G., McClelland, M., & Gal-Mor, O. (2015). Flagellin is
611 required for host cell invasion and normal *Salmonella* Pathogenicity Island 1
612 expression by *Salmonella enterica* serovar Paratyphi A. *Infect Immun, 83*(9), 3355-
613 3368. doi:10.1128/IAI.00468-15
614 Forest, C. G., Ferraro, E., Sabbagh, S. C., & Daigle, F. (2010). Intracellular survival of
615 *Salmonella enterica* serovar Typhi in human macrophages is independent of
616 *Salmonella* pathogenicity island (SPI)-2. *Microbiology, 156*(Pt 12), 3689-3698.
617 doi:10.1099/mic.0.041624-0
618 Gal-Mor, O. (2019). Persistent infection and long-term carriage of typhoidal and nontyphoidal
619 Salmonellae. *Clin Microbiol Rev, 32*(1). doi:10.1128/CMR.00088-18
620 Hansen-Wester, I., Stecher, B., & Hensel, M. (2002). Type III secretion of *Salmonella*
621 *enterica* serovar Typhimurium translocated effectors and SseFG. *Infect. Immun., 70*(3), 1403-1409. doi:10.1128/iai.70.3.1403-1409.2002.
623 Helaine, S., & Holden, D. W. (2013). Heterogeneity of intracellular replication of bacterial
624 pathogens. *Curr Opin Microbiol, 16*(2), 184-191. doi:10.1016/j.mib.2012.12.004
625 Hensel, M., Shea, J. E., Gleeson, C., Jones, M. D., Dalton, E., & Holden, D. W. (1995).
626 Simultaneous identification of bacterial virulence genes by negative selection.
627 *Science, 269*(5222), 400-403. doi:10.1126/science.7618105.
628 Hensel, M., Shea, J. E., Waterman, S. R., Mundy, R., Nikolaus, T., Banks, G., . . . Holden, D.
629 W. (1998). Genes encoding putative effector proteins of the type III secretion system
630 of *Salmonella* pathogenicity island 2 are required for bacterial virulence and
631 proliferation in macrophages. *Mol Microbiol, 30*(1), 163-174. doi:10.1046/j.1365-
632 2958.1998.01047.x
633 Hoffmann, S., Schmidt, C., Walter, S., Bender, J. K., & Gerlach, R. G. (2017). Scarless
634 deletion of up to seven methyl-accepting chemotaxis genes with an optimized method
635 highlights key function of CheM in *Salmonella* Typhimurium. *PLoS One, 12*(2),
636 e0172630. doi:10.1371/journal.pone.0172630
637 Holt, K. E., Thomson, N. R., Wain, J., Langridge, G. C., Hasan, R., Bhutta, Z. A., . . .
638 Parkhill, J. (2009). Pseudogene accumulation in the evolutionary histories of
639 *Salmonella enterica* serovars Paratyphi A and Typhi. *BMC Genomics, 10*, 36.
640 doi:10.1186/1471-2164-10-36
641 Jennings, E., Thurston, T. L. M., & Holden, D. W. (2017). *Salmonella* SPI-2 Type III
642 secretion system effectors: molecular mechanisms and physiological consequences.
643 *Cell Host Microbe, 22*(2), 217-231. doi:10.1016/j.chom.2017.07.009
644 Karlinsey, J. E., Stepien, T. A., Mayho, M., Singletary, L. A., Bingham-Ramos, L. K., Brehm,
645 M. A., . . . Fang, F. C. (2019). Genome-wide analysis of *Salmonella enterica* serovar
646 Typhi in humanized mice reveals key virulence features. *Cell Host Microbe, 26*(3),
647 426-434 e426. doi:10.1016/j.chom.2019.08.001
648 Knodler, L. A., Vallance, B. A., Celli, J., Winfree, S., Hansen, B., Montero, M., & Steele-
649 Mortimer, O. (2010). Dissemination of invasive *Salmonella* via bacterial-induced
650 extrusion of mucosal epithelia. *Proc. Natl. Acad. Sci. U S A, 107*(41), 17733-17738.
651 doi:1006098107 [pii] 10.1073/pnas.1006098107
652 Knodler, L. A., Vallance, B. A., Hensel, M., Jackel, D., Finlay, B. B., & Steele-Mortimer, O.
653 (2003). *Salmonella* type III effectors PipB and PipB2 are targeted to detergent-

654 resistant microdomains on internal host cell membranes. *Mol Microbiol, 49*(3), 685-
655 704. doi:10.1046/j.1365-2958.2003.03598.x
656 Krieger, V., Liebl, D., Zhang, Y., Rajashekar, R., Chlanda, P., Giesker, K., . . . Hensel, M.
657 (2014). Reorganization of the endosomal system in *Salmonella*-infected cells: the
658 ultrastructure of *Salmonella*-induced tubular compartments. *PLoS Pathog, 10*(9),
659 e1004374. doi:10.1371/journal.ppat.1004374
660 Kuhle, V., & Hensel, M. (2002). SseF and SseG are translocated effectors of the type III
661 secretion system of *Salmonella* pathogenicity island 2 that modulate aggregation of
662 endosomal compartments. *Cell. Microbiol., 4*(12), 813-824. Retrieved from 12464012
663 Lewis, K. (2010). Persister cells. *Annu Rev Microbiol, 64*, 357-372.
664 doi:10.1146/annurev.micro.112408.134306
665 Liss, V., Swart, A. L., Kehl, A., Hermanns, N., Zhang, Y., Chikkaballi, D., . . . Hensel, M.
666 (2017). *Salmonella enterica* remodels the host cell endosomal system for efficient
667 intravacuolar nutrition. *Cell Host Microbe, 21*(3), 390-402.
668 doi:10.1016/j.chom.2017.02.005
669 Löber, S., Jäckel, D., Kaiser, N., & Hensel, M. (2006). Regulation of *Salmonella*
670 pathogenicity island 2 genes by independent environmental signals. *Int. J. Med.*
671 *Microbiol., 296*(7), 435-447. doi:10.1016/j.ijmm.2006.05.001.
672 McClelland, M., Sanderson, K. E., Clifton, S. W., Latreille, P., Porwollik, S., Sabo, A., . . .
673 Wilson, R. K. (2004). Comparison of genome degradation in Paratyphi A and Typhi,
674 human-restricted serovars of *Salmonella enterica* that cause typhoid. *Nat Genet,*
675 *36*(12), 1268-1274. Retrieved from 15531882
676 McDowell, M. A., Byrne, A. M., Mylona, E., Johnson, R., Sagfors, A., Crepin, V. F., . . .
677 Frankel, G. (2019). The *S.* Typhi effector StoD is an E3/E4 ubiquitin ligase which
678 binds K48- and K63-linked diubiquitin. *Life Sci Alliance, 2*(3).
679 doi:10.26508/lsa.201800272
680 Noster, J., Chao, T. C., Sander, N., Schulte, M., Reuter, T., Hansmeier, N., & Hensel, M.
681 (2019). Proteomics of intracellular *Salmonella enterica* reveals roles of *Salmonella*
682 pathogenicity island 2 in metabolism and antioxidant defense. *PLoS Pathog, 15*(4),
683 e1007741. doi:10.1371/journal.ppat.1007741
684 Obert, S., O'Connor, R. J., Schmid, S., & Hearing, P. (1994). The adenovirus E4-6/7 protein
685 transactivates the E2 promoter by inducing dimerization of a heteromeric E2F
686 complex. *Mol. Cell Biol., 14*(2), 1333-1346. Retrieved from 8289811
687 Ochman, H., Soncini, F. C., Solomon, F., & Groisman, E. A. (1996). Identification of a
688 pathogenicity island required for *Salmonella* survival in host cells. *Proc Natl Acad Sci*
689 *U S A, 93*(15), 7800-7804. doi:10.1073/pnas.93.15.7800
690 Prouty, A. M., Schwesinger, W. H., & Gunn, J. S. (2002). Biofilm formation and interaction
691 with the surfaces of gallstones by *Salmonella* spp. *Infect Immun, 70*(5), 2640-2649.
692 doi:10.1128/iai.70.5.2640-2649.2002
693 Rajashekar, R., Liebl, D., Chikkaballi, D., Liss, V., & Hensel, M. (2014). Live cell imaging
694 reveals novel functions of *Salmonella enterica* SPI2-T3SS effector proteins in
695 remodeling of the host cell endosomal system. *PLoS One, 9*(12), e115423.
696 doi:10.1371/journal.pone.0115423
697 Rajashekar, R., Liebl, D., Seitz, A., & Hensel, M. (2008). Dynamic remodeling of the
698 endosomal system during formation of *Salmonella*-induced filaments by intracellular
699 *Salmonella enterica*. *Traffic, 9*(12), 2100-2116. doi:TRA821 [pii] 10.1111/j.1600-
700 0854.2008.00821.x
701 Röder, J., & Hensel, M. (2020). Presence of SopE and mode of infection result in increased
702 *Salmonella*-containing vacuole damage and cytosolic release during host cell infection
703 by *Salmonella enterica*. *Cell Microbiol, 22*(5), e13155. doi:10.1111/cmi.13155

Saleh, S., Van Puyvelde, S., Staes, A., Timmerman, E., Barbe, B., Jacobs, J., . . . Deborggraeve, S. (2019). *Salmonella* Typhi, Paratyphi A, Enteritidis and Typhimurium core proteomes reveal differentially expressed proteins linked to the cell surface and pathogenicity. *PLoS Negl Trop Dis, 13*(5), e0007416. doi:10.1371/journal.pntd.0007416

Schulte, M., Olschewski, K., & Hensel, M. (2020). Fluorescent protein-based reporters reveal stress response of intracellular Salmonella enterica at level of single bacterial cells. *Cell Microbiol, in revision*. doi:10.1111/cmi.13293

Schulte, M., Sterzenbach, T., Miskiewicz, K., Elpers, L., Hensel, M., & Hansmeier, N. (2019). A versatile remote control system for functional expression of bacterial virulence genes based on the *tetA* promoter. *Int J Med Microbiol, 309*(1), 54-65. doi:10.1016/j.ijmm.2018.11.001

Sepe, L. P., Hartl, K., Iftekhar, A., Berger, H., Kumar, N., Goosmann, C., . . . Boccellato, F. (2020). Genotoxic effect of *Salmonella* Paratyphi A infection on human primary gallbladder cells. *mBio, 11*(5). doi:10.1128/mBio.01911-20

Shea, J. E., Hensel, M., Gleeson, C., & Holden, D. W. (1996). Identification of a virulence locus encoding a second type III secretion system in *Salmonella typhimurium*. *Proc Natl Acad Sci U S A, 93*(6), 2593-2597. doi:10.1073/pnas.93.6.2593

Sorensen, M., Lippuner, C., Kaiser, T., Misslitz, A., Aebischer, T., & Bumann, D. (2003). Rapidly maturing red fluorescent protein variants with strongly enhanced brightness in bacteria. *FEBS Lett, 552*(2-3), 110-114. doi:10.1016/s0014-5793(03)00856-1

St-Pierre, F., Cui, L., Priest, D. G., Endy, D., Dodd, I. B., & Shearwin, K. E. (2013). One-step cloning and chromosomal integration of DNA. *ACS Synth Biol, 2*(9), 537-541. doi:10.1021/sb400021j

Stapels, D. A. C., Hill, P. W. S., Westermann, A. J., Fisher, R. A., Thurston, T. L., Saliba, A. E., . . . Helaine, S. (2018). *Salmonella* persisters undermine host immune defenses during antibiotic treatment. *Science, 362*(6419), 1156-1160. doi:10.1126/science.aat7148

Stein, M. A., Leung, K. Y., Zwick, M., Garcia-del Portillo, F., & Finlay, B. B. (1996). Identification of a *Salmonella* virulence gene required for formation of filamentous structures containing lysosomal membrane glycoproteins within epithelial cells. *Mol Microbiol, 20*(1), 151-164. doi:10.1111/j.1365-2958.1996.tb02497.x

Tomljenovic-Berube, A. M., Mulder, D. T., Whiteside, M. D., Brinkman, F. S., & Coombes, B. K. (2010). Identification of the regulatory logic controlling *Salmonella* pathoadaptation by the SsrA-SsrB two-component system. *PLoS Genet., 6*(3), e1000875. doi:10.1371/journal.pgen.1000875

Vorwerk, S., Krieger, V., Deiwick, J., Hensel, M., & Hansmeier, N. (2015). Proteomes of host cell membranes modified by intracellular activities of *Salmonella enterica*. *Mol Cell Proteomics, 14*(1), 81-92. doi:10.1074/mcp.M114.041145

Walawalkar, Y. D., Vaidya, Y., & Nayak, V. (2016). Response of *Salmonella* Typhi to bile-generated oxidative stress: implication of quorum sensing and persister cell populations. *Pathog Dis, 74*(8). doi:10.1093/femspd/ftw090

Tables

Table 1. Bacterial strains used in this study

Designation	relevant characteristics	reference
S. enterica serovar Typhimurium		
NCTC12023	wild type	Lab collection
P2D6	*ssaV*::mTn*5*	(Shea et al., 1996)
MvP503	Δ*sifA*::FRT	(Kuhle & Hensel, 2002)
S. enterica serovar Typhi		
120130191	wild type	clinical isolate, SalHostTrop consortium
STY101	Δ*ssaR*::*aph*	this study
STY118	Δ*ssaR*::FRT	this study
STY110	Δ*sifA*::*aph*	this study
STY123	Δ*sifA*::FRT	this study
STY132	Δ*ssrB*::*aph*	this study
STY134	Δ*ssaK*::*aph*	this study
STY137	Δ*ssaK*::FRT	this study
S. enterica serovar Paratyphi A		
45157	wild type	clinical isolate, SalHostTrop consortium
SPA118	Δ*ssaR*::FRT	this study
SPA110	Δ*sifA*::*aph*	this study
SPA132	Δ*ssrB*::*aph*	this study

769 Table 2. Plasmids used in this study

Designation	relevant characteristics	reference
pFPV-mCherry	const. mCherry	(Drecktrah et al., 2008)
pWRG167	P_{EM7}::sfGFP in pWRG81	(Bender, Wille, Blank, Lange, & Gerlach, 2013)
pMW211	const. DsRed T3_S4T	(Sorensen et al., 2003)
pWRG730	Red recombinase expression	(Hoffmann, Schmidt, Walter, Bender, & Gerlach, 2017)
pE-FLP	FLP recombinase expression	(St-Pierre et al., 2013)
pGL-Rab7 wt	Rab7a::GFP	(Vorwerk, Krieger, Deiwick, Hensel, & Hansmeier, 2015)
p2095	P_{sseA} *sscB sseF*::M45	(Hansen-Wester et al., 2002)
p2129	P_{sseJ} *sseJ*::M45	(Hansen-Wester et al., 2002)
p2621	P_{pipB2} *pipB2*::M45	(Knodler et al., 2003)
p3301	P_{sseL} *sseL*::HA	Lab collection
p3774	const. RFP	Lab collection
p3776	P_{EM7}::RFP P_{ssaG}::sfGFP	(Röder & Hensel, 2020)
p4514	Arl8A::eGFP	this study
p4889	P_{EM7}::DsRed P_{uhpT}::sfGFP	(Röder & Hensel, 2020)
p4928	P_{EM7}::RFP *tetR* P_{tetA}::sfGFP	(Schulte et al., 2019)

789

790

Figure and Figure Legends

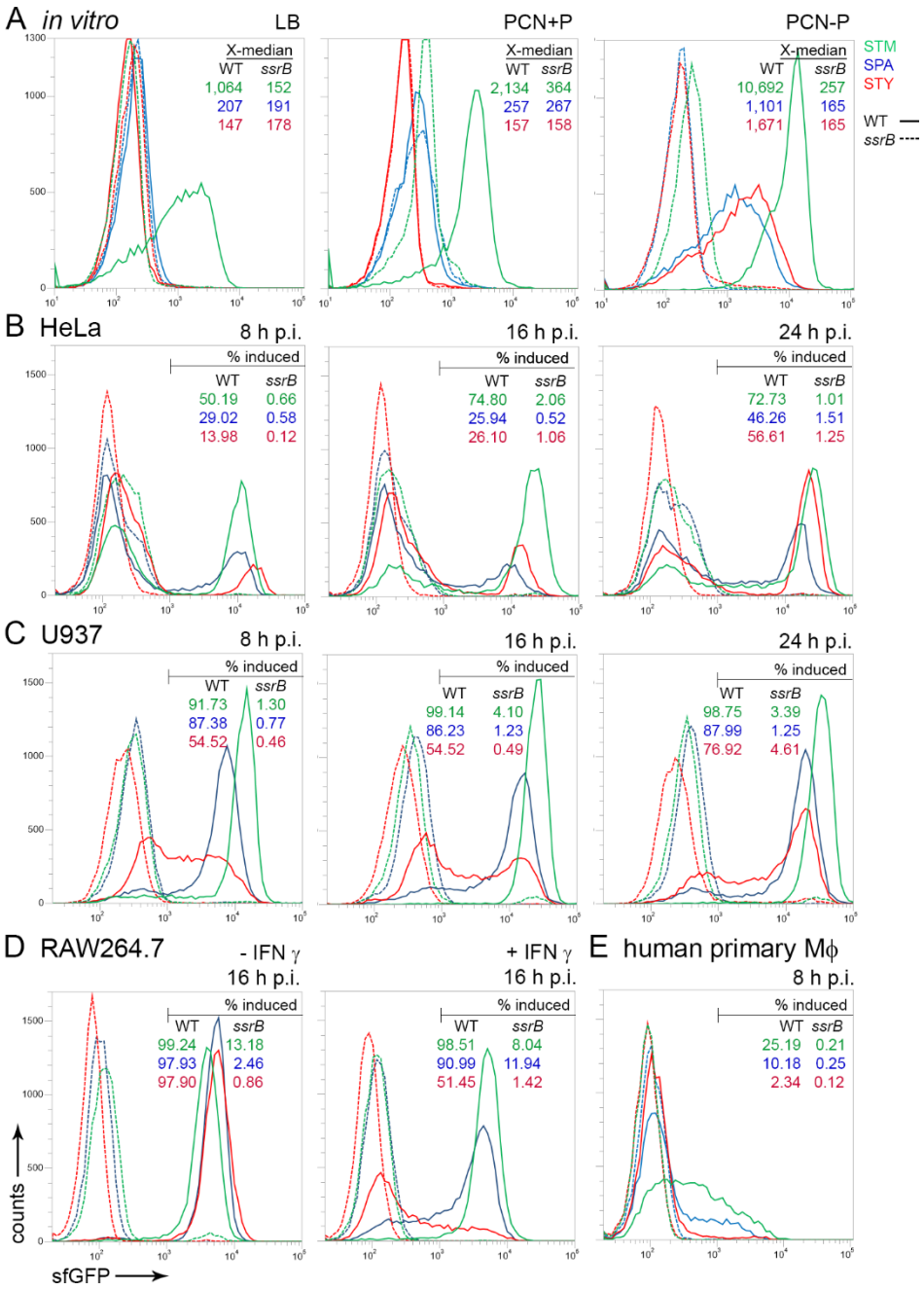

Fig. 1. Expression of genes encoding the SPI2-T3SS by intracellular STM, SPA and STY. STM (green), SPA (blue), or STY (red) WT (solid lines) or *ssrB* mutant (dashed lines) strains were used, all harboring plasmid p3776 for constitutive expression of DsRed, and sfGFP under control of the *ssaG* promoter. **A**) Various strains were grown in non-inducing PCN medium (PCN pH 7.4, 25 mM P_i), or inducing PCN medium (PCN pH 5.8, 0.4 mM P_i). After culture o/n with aeration by rotation at 60 rpm in a roller drum, aliquots of cultures were fixed, and

bacteria were analyzed by flow cytometry (FC). The x -median values for the sfGFP-positive bacteria are indicated. Various strains were used to infect HeLa cells (**B**), U937 macrophages (**C**), RAW264.7 macrophages (**D**) without or with activation by γ-interferon (IFN γ), or human primary macrophages (**E**). At 8 h, 16 h, or 24 h p.i. as indicated, host cells were lysed in order to release bacteria. For FC, at least 10,000 bacteria-sized particles with DsRed fluorescence were gated and GFP intensities were quantified. The percentage of intracellular bacteria with induction of P_{ssaG}::sfGFP is indicated for WT and Δ*ssrB* strains. The data set shown is representative for three independent experiments with similar outcome.

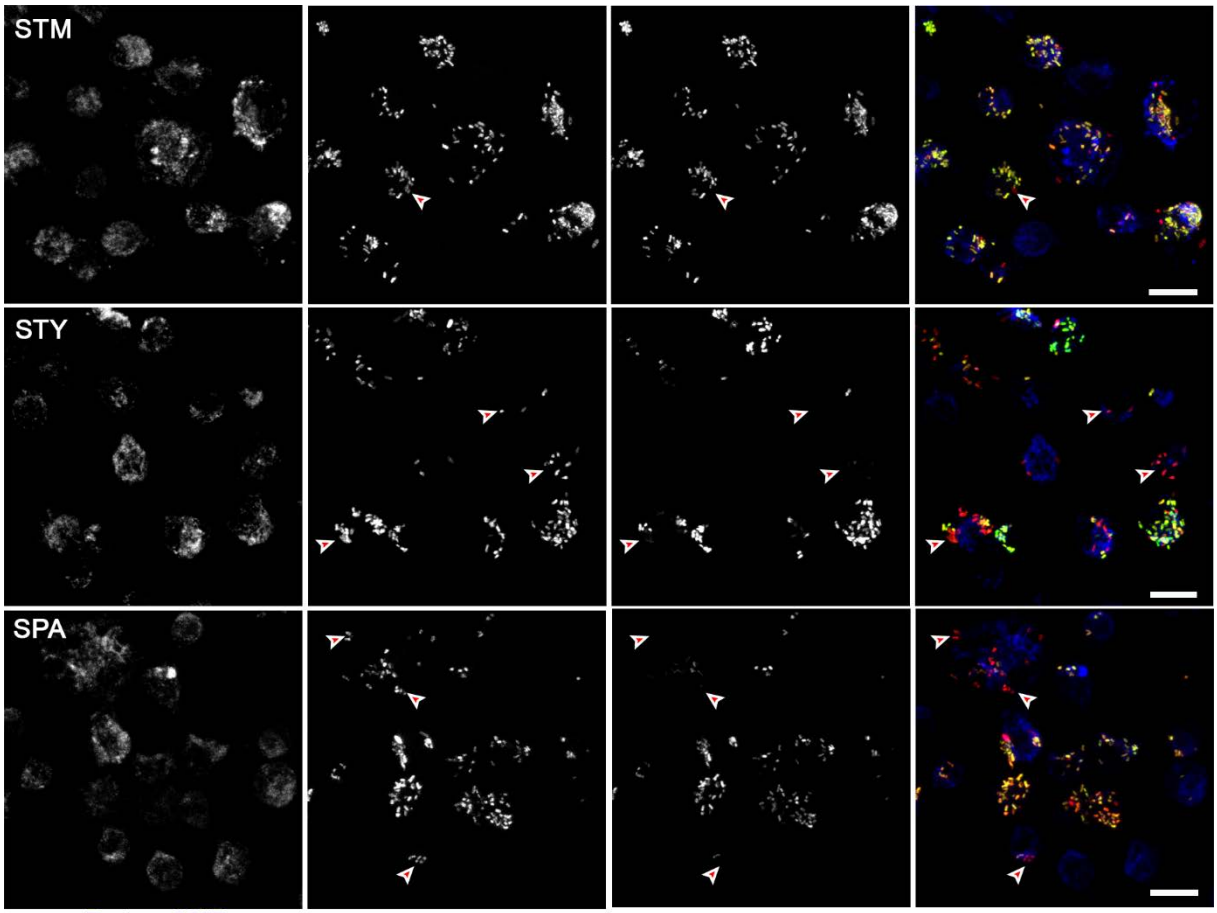

Fig. 2. Heterogeneity of P_{ssaG} induction by intracellular STM, SPA and STY. U937 cells were infected at MOI 50 with STM, STY, or SPA WT strains all harboring plasmid p3776 for constitutive expression of RFP (red), and sfGFP (green) under control of the *ssaG* promoter. To label the endosomal system, cells were pulsed with dextran-Alexa647 (dextran-A647, blue) from 1 h p.i. until fixation. Cells were fixed with PFA 8 h p.i. and microscopy was performed by CLSM on a Leica SP5 using a 40x objective. Red arrowheads indicate representative, P_{ssaG}::sfGFP-negative intracellular *Salmonella*. Scale bars: 10 µm.

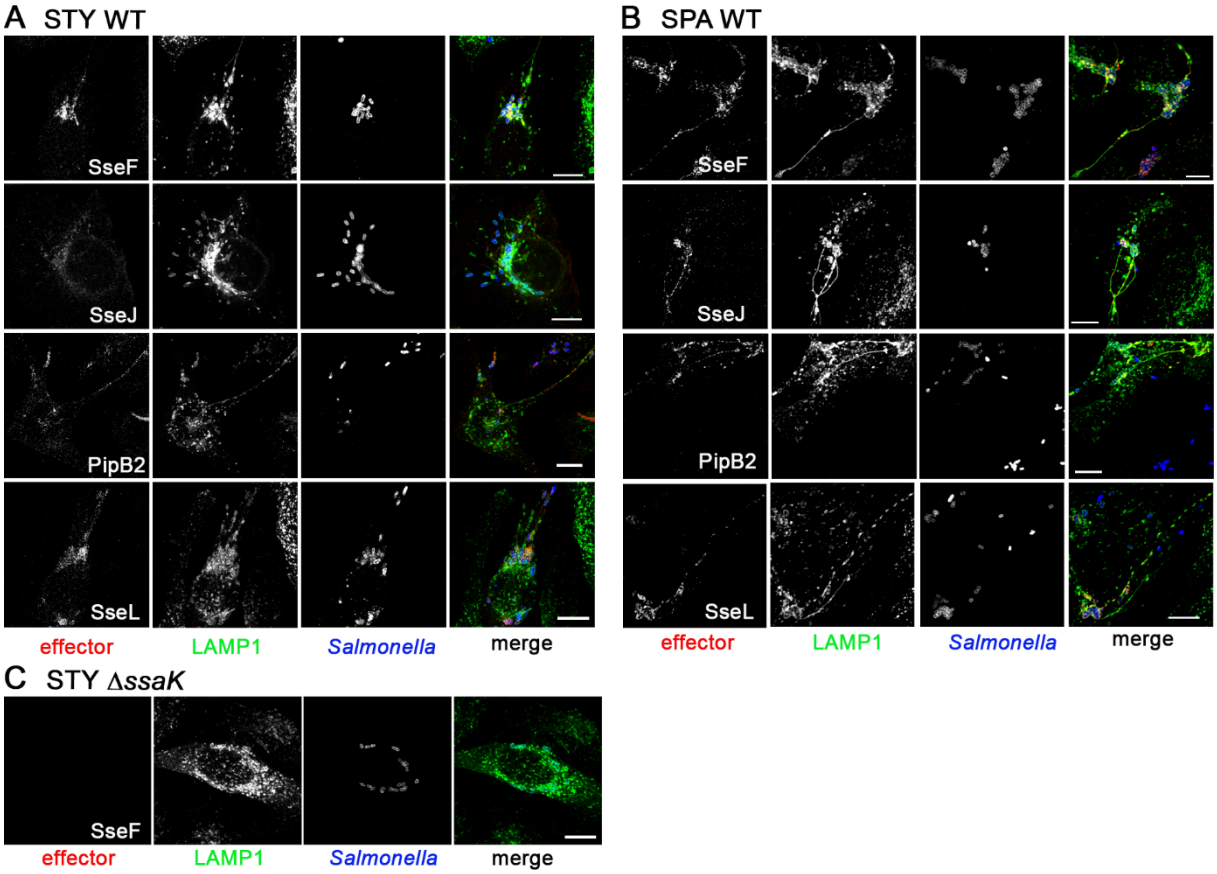

Fig. 3. The SPI2-T3SS of SPA and STY is functional in translocation of effector proteins. HeLa cells constitutively expressing LAMP1-GFP (green) were infected with STY WT (**A**) or SPA WT (**B**) harboring plasmids for expression of *sseF*::M45, *sseJ*::M45, *pipB2*::M45, or *sseL*::HA as indicated. At 9 h p.i., cells were fixed, permeabilized by Saponin and immunolabeled for M45 or HA epitope tags (red) to localize translocated effector proteins, and with serovar-specific anti O-Ag antibodies to label bacteria (blue). **C**) Micrographs of cells infected with SPI2-T3SS-defcient STY strain Δ*ssaK* harboring a plasmid for expression of *sseF*::M45. Microscopy was performed by CLSM using a Leica SP5 with 100x objective. Scale bars: 10 µm.

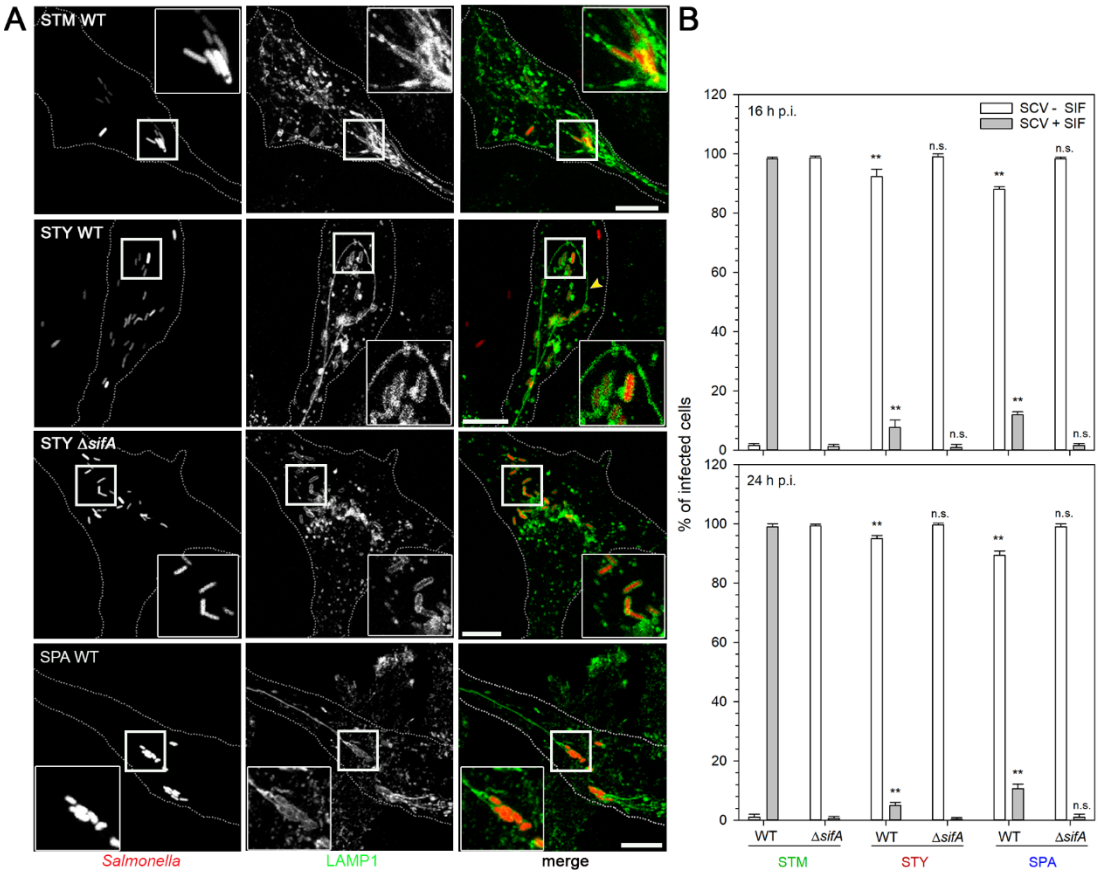

Fig. 4. Endosomal remodeling in host cells infected with STM, SPA, or STY is dependent on function of SifA. A) HeLa LAMP1-GFP cells were infected with WT or Δ*sifA* strains of STM, STY or SPA as indicated, constitutively expression mCherry (red) at MOI 50. Cells were fixed at 8 h p.i. and microscopy was performed by CLSM on a Leica SP5 using a 40x objective. Scale bar, 10 µm. **B**) Quantification of SIF formation in HeLa cell infected by STM, STY, or SPA. HeLa LAMP1-GFP cells were infected with WT or *sifA* mutant strains of STM, STY, or SPA at MOI 50. Cell were fixed 16 or 24 h p.i., and microscopy was performed with CLSM using a Leica SP5 with 40x objective. At least 100 cells per strain and time point were counted, and infected cells were scored for appearance of SIF. Statistical analysis was performed by One-way ANOVA and are indicated as follows: n.s., not significant; *, $P < 0.05$; **, $P < 0.001$.

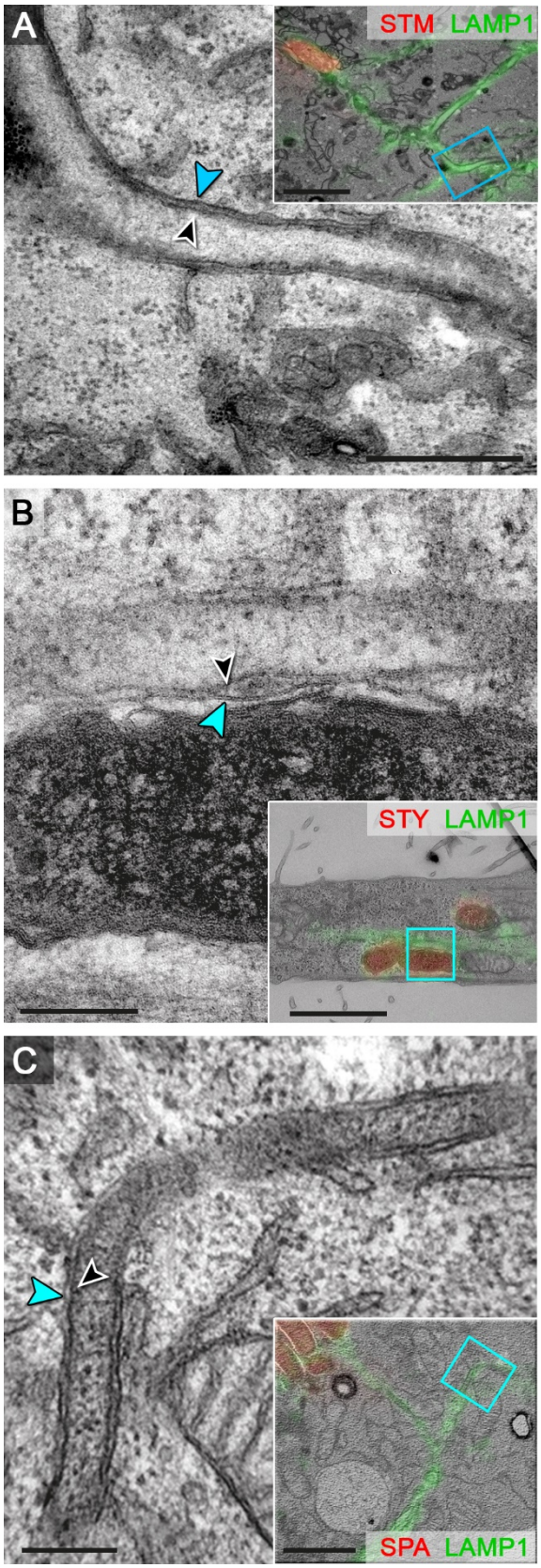

Fig. 5. Ultrastructure of endosomal compartments remodeled by intracellular STM, STY, or SPA. HeLa cells expressing LAMP1-GFP (green) were infected with STM (**A**), STY (**B**),

or SPA (**C**) WT, each expressing mCherry (red). Cell were fixed 7 h p.i. and processed for confocal fluorescence microscopy (FM) and transmission electron microscopy (TEM) of ultrathin sections. FM and TEM modalities were superimposed (inserts) for correlation, and details of the ultrastructure of tubular LAMP1-positive membrane compartment are shown at higher magnification. Double membrane SIF with inner (black arrowhead) and outer (blue arrowhead) membrane. Scale bars: 200 nm (details), 2 µm (inserts for overview).

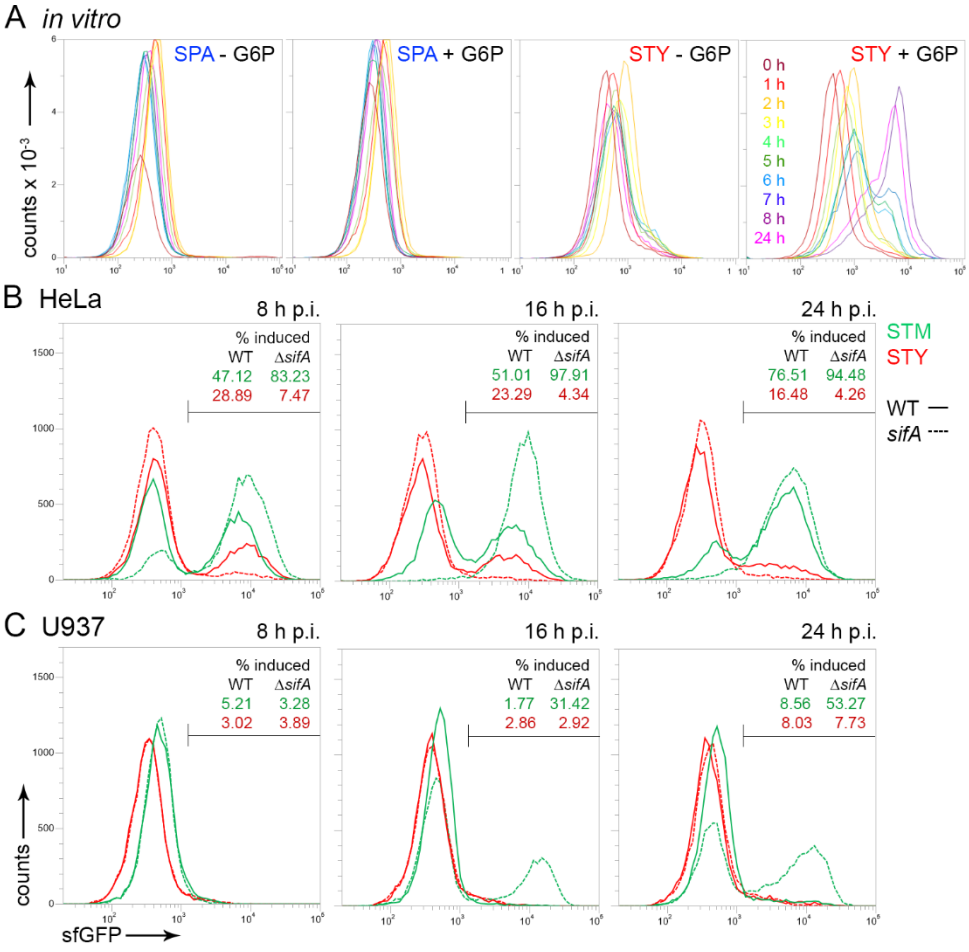

Fig. 6. SCV integrity and cytosolic release of STM and STY. STM (green), SPA (blue), or STY (red), WT (solid lines) or Δ*sifA* (dashed lines) strains were used as indicated, each harboring plasmid p4889 for constitutive expression of DsRed, and P_{uhpT}-controlled expression of sfGFP as sensor for cytosolic exposure. **A)** Induction of P_{uhpT}::sfGFP by glucose-6-phosphate (G6P) in SPA and STY. SPA or STY WT harboring p4889 were grown in LB broth without or with addition of 0.2% G6P. Samples were collected at various time points of subculture as indicated by various colors. Bacteria constitutively expressing DsRed were analysed by FC for levels of sfGFP expression. **B, C)** WT (solid lines) or *sifA* mutant (dashed lines) strains of STM (green) or STY (red), each harboring plasmid p4889 were used to infect HeLa cells (**B**), or U937 cells (**C**). At 8 h, 16 h, or 24 h p.i. as indicated, host cells were lysed in order to release bacteria. For FC, at least 10,000 bacteria-sized particles with DsRed fluorescence were gated and the GFP intensity was quantified. The percentage of bacterial cells with induction of

863 P_{uphT}::sfGFP is indicated for WT and *sifA* mutant strains. The data sets shown are representative

864 for three independent experiments with similar outcome.

865

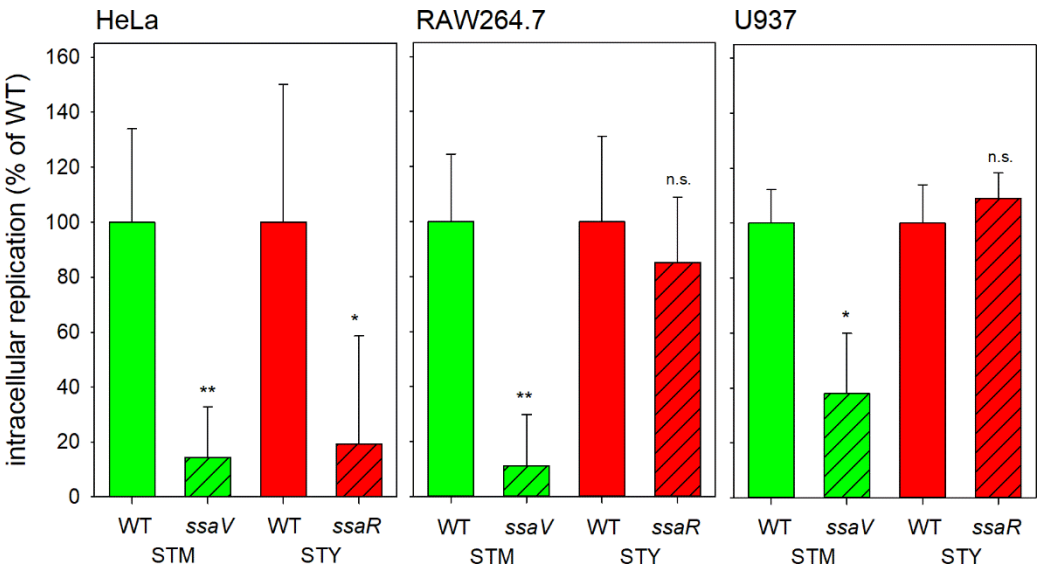

Fig. 7. SPI2-T3SS-deficient STY are reduced in intracellular replication in HeLa cells. Hosts cells were infected with WT (open bars) or SPI2-T3SS-deficient (hatched bars, *ssaV* and *ssaR* encode subunits of the SPI2-T3SS) strains of STM (green) or STY (red) at MOI 1. Intracellular replication was determined by gentamicin protection assays comparing intracellular CFU recovered 1 h p.i. and 24 h p.i. **A)** Intracellular replication in HeLa cells**.** STM was cultured overnight, diluted 1:31 in fresh LB broth, subcultured 2.5 h, and used for infection. STY was incubated in 3 ml LB broth for 8 h, reinoculated 1:100 in 10 ml fresh LB broth and grown for 16 h under microaerophilic conditions before use as inoculum in infection **B, C)** Bacterial strains were grown overnight in LB and aliquots were used to infect macrophages. **B)** Intracellular replication of STM and STY in RAW264.7 macrophages. **C)** Intracellular replication of STM and STY in U937 cells. Assays were performed in three biological replicates, and one representative assay is shown. Student´s *t*-test was used for statistical analysis and significance is indicated as follows: n.s., not significant; *, P > 0.05; **, P > 0.01.

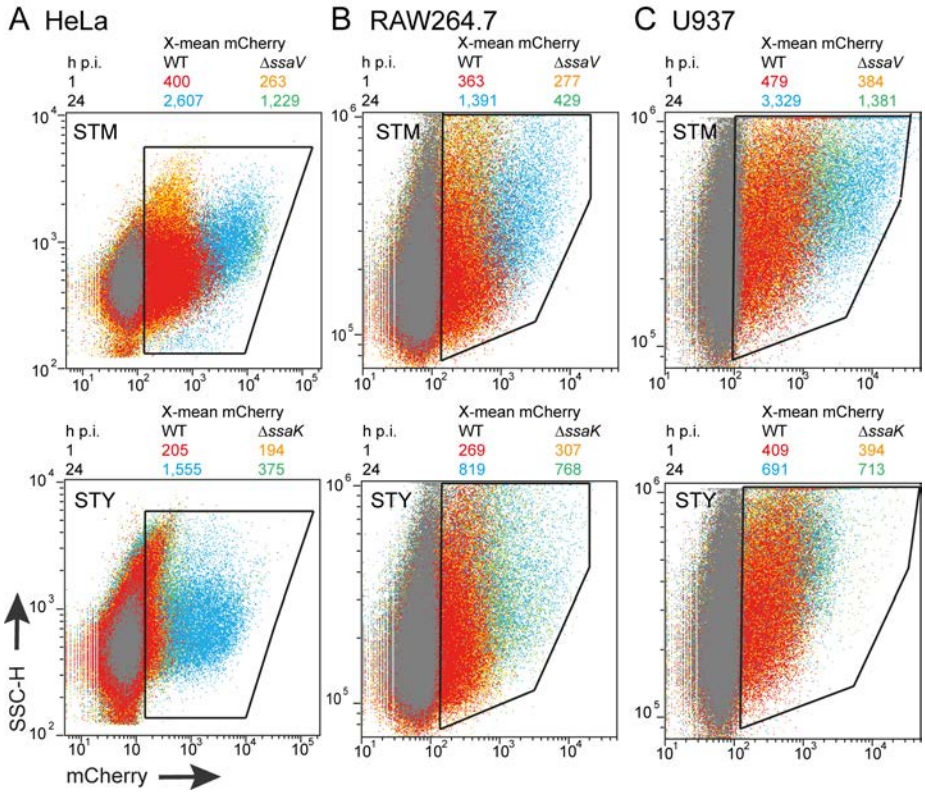

881

882 **Fig. 8. Intracellular proliferation of STM and STY in HeLa cells, RAW264.7**
883 **macrophages, or U937 macrophages determined flow cytometry.** For infection of HeLa
884 cells (**A**) STM was cultured overnight in 3 ml LB broth and reinoculated 1:31 in fresh LB broth
885 for 3.5 h. STY was incubated in 3 ml LB broth for 8 h and reinoculated 1:100 in 10 ml fresh
886 LB broth for 16 h under microaerophilic conditions. For infection of RAW264.7 macrophages
887 (**B**), or U937 macrophages (**C**), overnight cultures were used. At 1 h or 24 h p.i. as indicated,
888 cells were washed, fixed and detached. The cell populations were analysed by flow cytometry
889 and gating was set to cells harboring intracellular *Salmonella* as indicated by polygons. At least
890 10,000 *Salmonella*-infected host cells were scored. Overlays of dot plots show WT *Salmonella*
891 at 1 h or 24 h p.i. in red and blue, respectively, and Δ*ssaV*/Δ*ssaK Salmonella* at 1 h or 24 h p.i.
892 in orange and green, respectively. The X-mean values for mCherry fluorescence intensities of
893 infected cells are shown in same colors above each overlay. Individual dot plots are shown in
894 **Fig. S 7**. Assays were performed in three biological replicates, one representative replicate is
895 shown.

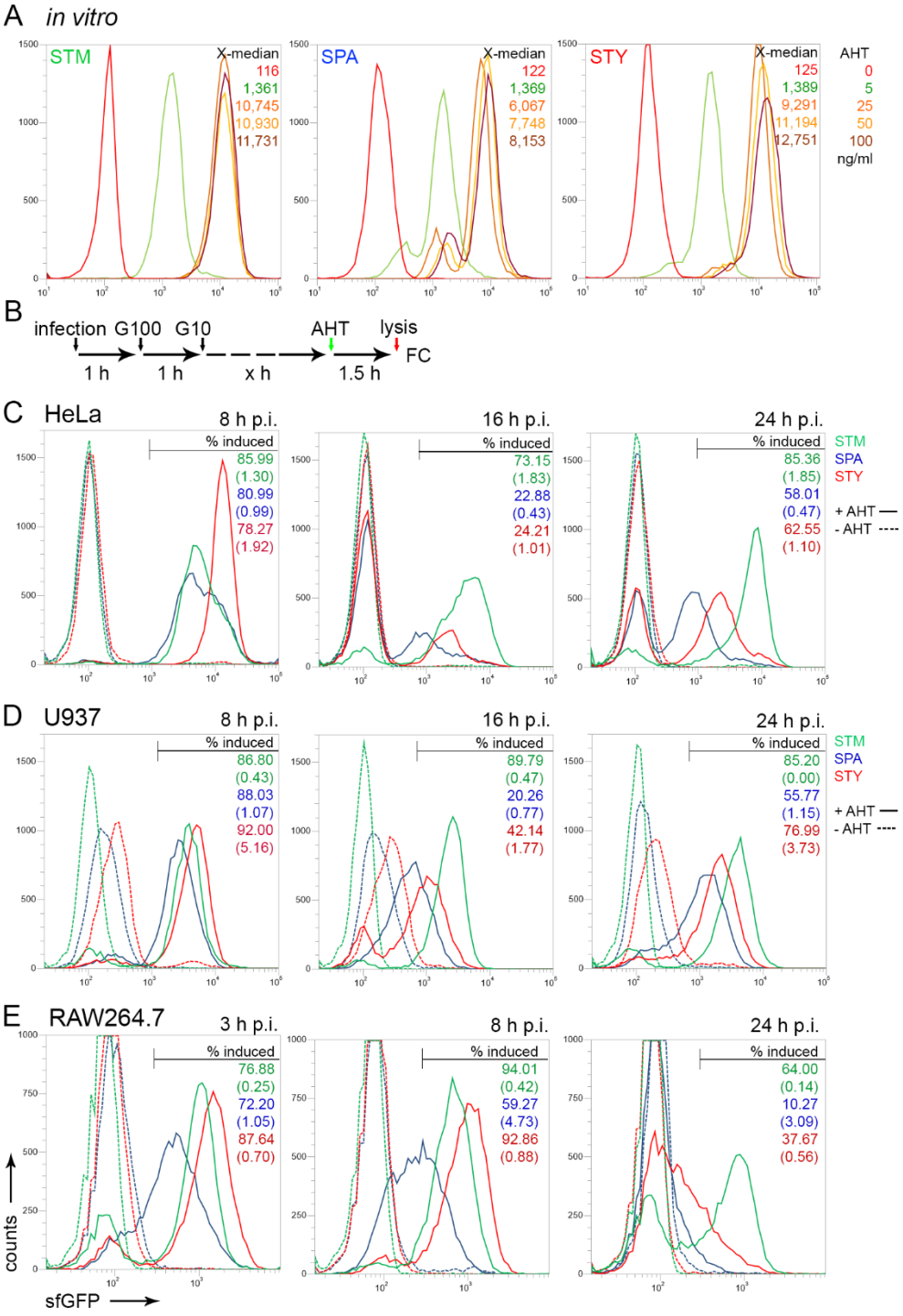

Fig. 9. Biosynthetic capability of intracellular STM, SPA and STY. A) STM (green), SPA (blue), and STY (red) WT strains, each harboring plasmid p4928 for constitutive expression of RFP, and sfGFP under control of the *tetA* promoter were subcultured in LB broth with aeration by rotation at 60 rpm in der roller drum. Various amounts of AHT as indicated were added after 1.5 h of culture. Culture was continued for 2 h, bacterial cells were fixed and the sfGFP fluorescence intensity was determined by FC for at least 50,000 DsRed-positive bacteria per

condition. The X-median values are shown for a representative experiment. **B**) STM, SPA, or STY WT strains harboring p4928 were used to infect HeLa cells (**C**), U937 cells (**D**), or RAW264.7 cells (**E**). After infection for 1 h, medium was exchanged against medium containing 100 µg x ml^{-1} gentamicin (G100) for 1 h, followed by medium containing 10 µg x ml^{-1} gentamicin for the rest of the experiment. For induction of sfGFP expression, 50 ng x ml^{-1} AHT was added to infected cells 1.5 h prior lysis of host cells. At the time points p.i. indicated, host cells were lysed in order to release intracellular bacteria. For FC, at least 10,000 bacteria-sized particles were gated based on DsRed fluorescence, and the sfGFP intensity was quantified. The percentage of sfGFP-positive bacteria is indicated and values in brackets show the non-induced controls. The data sets shown are representative for three independent experiments with similar outcome.

Suppl. Tables

Table S 1. Oligonucleotides used in this study

Designation	Sequence 5' – 3'
Red mutagenesis primer	
ssaK-Del13-For	TCTTCATGGAGCATTTGCTATGAGTTTTACTTCACTTCC TATTCCGGGGATCCGTCGACC
ssaK-Del13-Rev	CATTACGTAACCATTTCAGTAACGCGTTGAAATGACGAG ATGTAGGCTGGAGCTGCTTCG
ssaR Del13 For	ATAATAGCGTTCCAGGTCGTGTCATGAGAGATAC AGTATGATTCCGGGGATCCGTCGACC
ssaR Del13 Rev	GAATCATTCATGAAAAGCTCTGTACCAATTGCGCC AGTGTTGTAGGCTGGAGCTGCTTCG
STY ssrB Del13 For	ATATTATCTTAATTTTCGCGAGGGCAGCAAAATGAAAGAA ATTCCGGGGATCCGTCGACC
STY ssrB Del13 Rev	ACCAATGCTTAATACCATCGGATGCCCCTGGTTAATAATAT GTAGGCTGGAGCTGCTTCG
Check PCR primer	
ssaK-DelCheck-For	CGTATACTTTGGCCGAAGAC
ssaK-DelCheck-Rev	TCCTGTAACTCCTGGAGAGC
ssaR DelCheck For	TGGTGCGTATTACACGTTGG
ssaR DelCheck Rev	TGAGTCAAGGCCTGAACAAG
STY ssaR DelCheck For	CCCACAGGCAATCAACTCAC
STY-ssaR-DelCheck-Rev2	GTGAGTTGATTGCCTGTGGG
STY ssrB DelCheck For	GGGCAGACTGAATTGGTATG
STY ssrB DelCheck Rev	TAGCGTGGCGGCATTGATAC

941 Table S 2. Antisera and antibodies used in this study

942 Antibody or antiserum	Characteristics	Source or reference
943 Group B Factors 1, 4, 5, 12	Rabbit anti-STM O antiserum	BD Difco
944 Group D1 Factors 1,9,12	Rabbit anti-STY O antiserum	BD Difco
945 Group A Factors 1,2,12	Rabbit anti-SPA O antiserum	BD Difco
946 Anti-M45	Mouse anti-M45 epitope tag	(Obert, O'Connor, Schmid,
947 & Hearing, 1994)		
948 Anti-HA	Rat anti-HA epitope tag	Roche
949 Anti-mouse IgG Alexa 568	Goat anti-mouse IgG Alexa 568	Thermo Fischer
950 Anti-rat IgG Alexa 568	Goat anti-rat IgG Alexa 568	Thermo Fischer
951 Anti-rabbit IgG Cy5	Goat anti-rabbit IgG Cy5	Jackson ImmunoResearch
952 Anti-rat IgG Cy5	Goat anti-rat IgG Cy5	Jackson ImmunoResearch

953

Suppl. Figure and Figure Legends

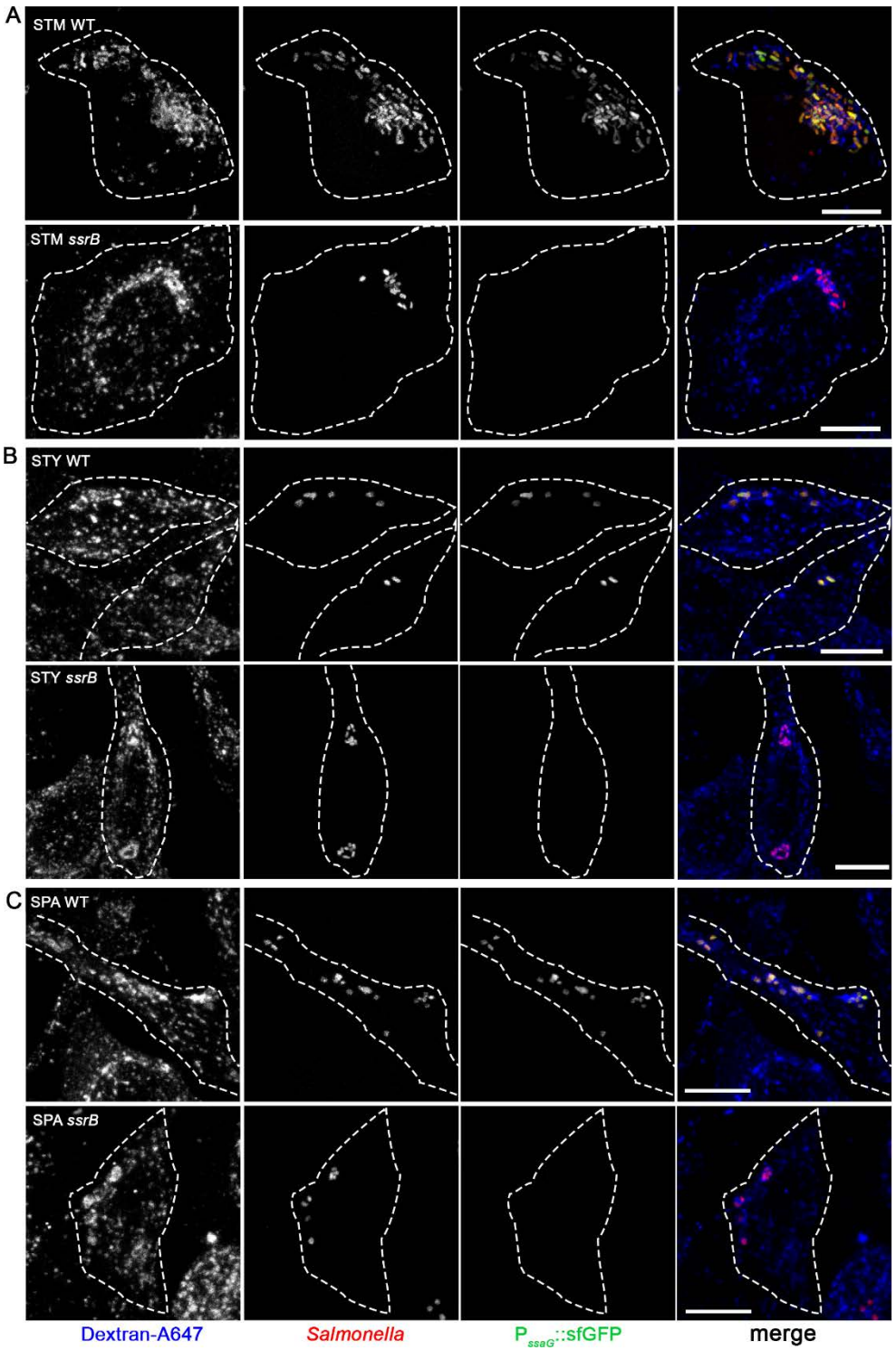

Fig. S 1. Induction of P_{ssaG} by intracellular STM, STY or SPA. HeLa cells were infected at MOI 75 with STM (**A**), STY (**B**), or SPA (**C**), WT or Δ*ssrB* strains all harboring plasmid p3776 for constitutive expression of RFP (red), and sfGFP (green) under control of the *ssaG* promoter.

959 To label the endosomal system, cells were pulsed with dextran-Alexa647 (dextran-A647, blue)
960 from 1 h p.i. until fixation. Cells were fixed with PFA 8 h p.i. and microscopy was performed
961 by CLSM on a Leica SP5 using the 100x objective. Scale bars, 10 µm
962

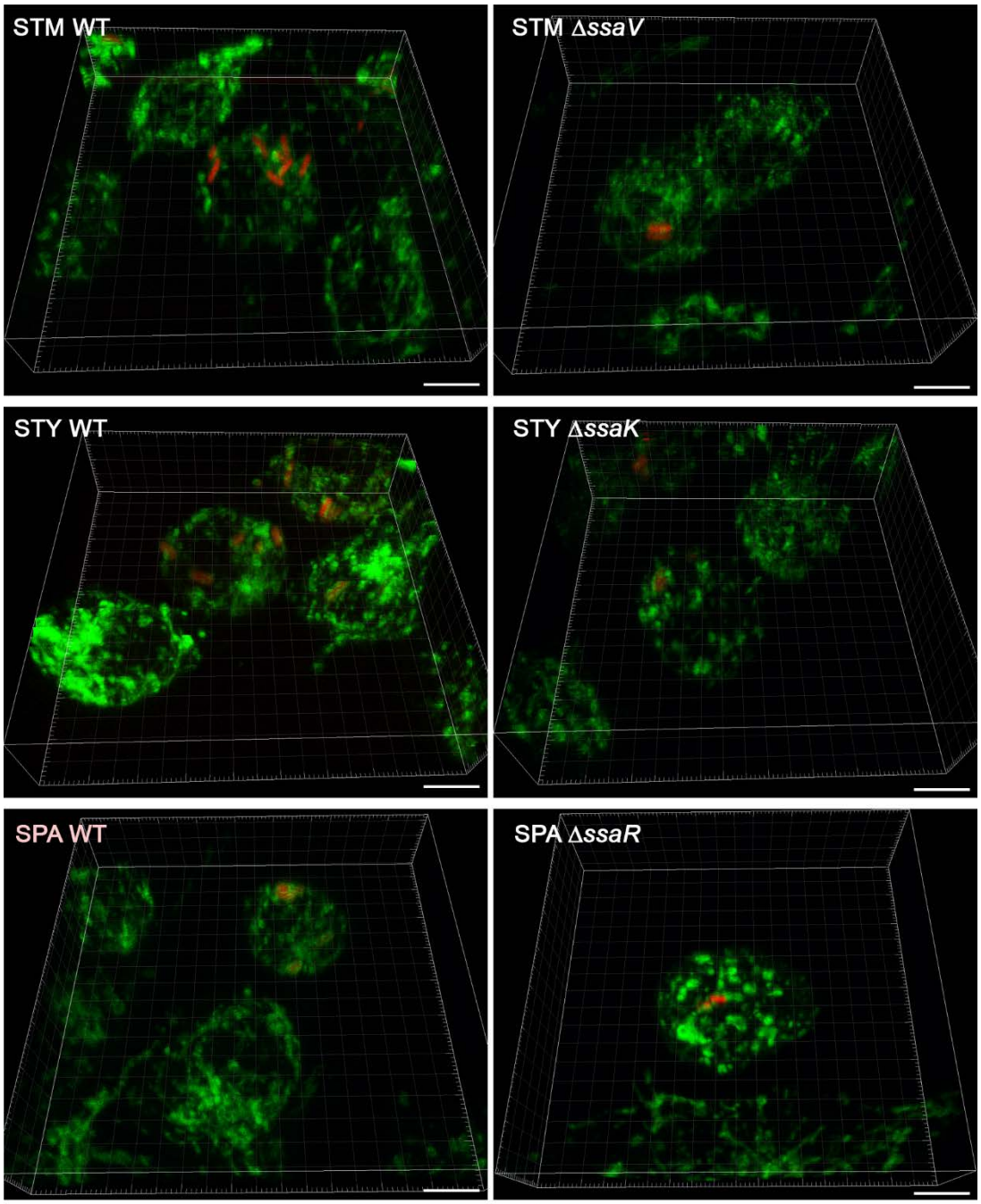

Fig. S 2. Formation of SCV in RAW264.7 macrophages infected with STM, STY, or SPA cells compared to STM. RAW264.7 cells constitutively expressing LAMP1-GFP were infected by WT or SPI2-T3SS-deficient strains (Δ*ssaV*, Δ*ssaK*, or Δ*ssaV*) of STM, STY, or SPA as indicated, each constitutively expressing mCherry. Cells were fixed 8 h p.i. and subjected to CLSM on a Leica SP5. 3D reconstructions of Z stacks are shown. Scale bars, 5 µm.

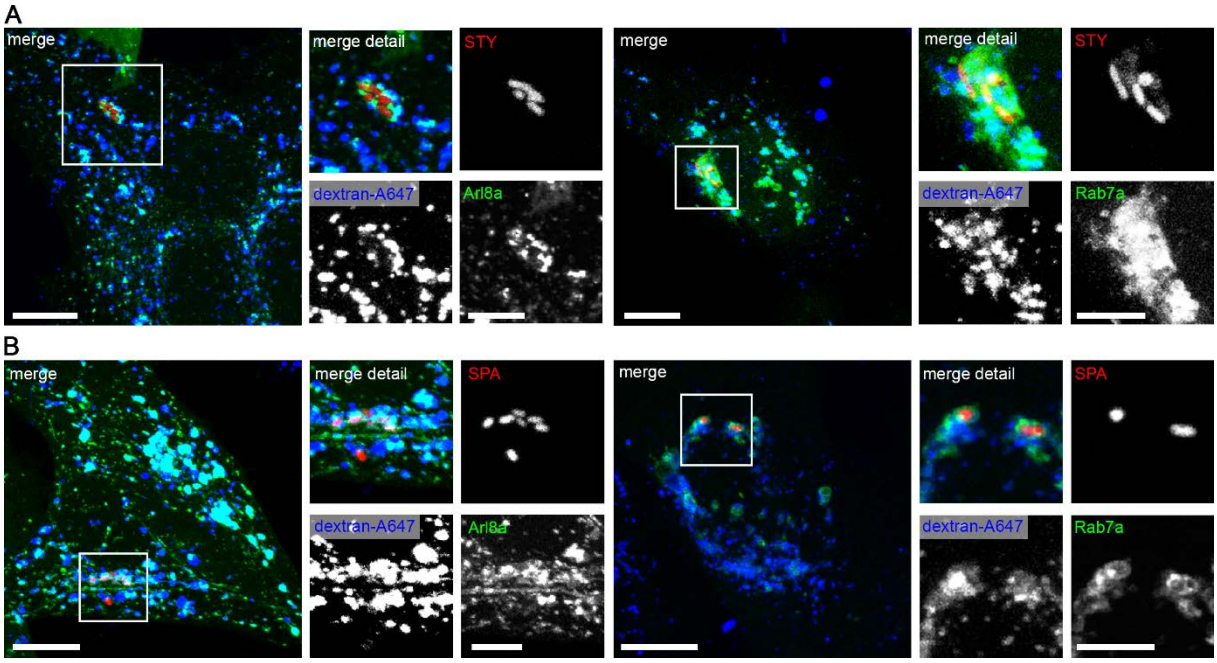

Fig. S 3. Vesicular compartments harboring STY or SPA are positive for canonical SCV markers Arl8A and Rab7. HeLa cells were transiently transfected with plasmids for the expression of Arl8A-eGFP or Rab7A-eGFP as indicated, and infected with STY (A) or SPA (B) at MOI 75 (for STY) or 50 (for SPA). Infected cells were pulsed-chased with Dextran-Alexa647 from 1 h p.i. until fixation. Microscopy was performed by CLSM on a Leica SP5 using a 100 x objective. Scale bars, 10 µm (overview); 5 µm (detail).

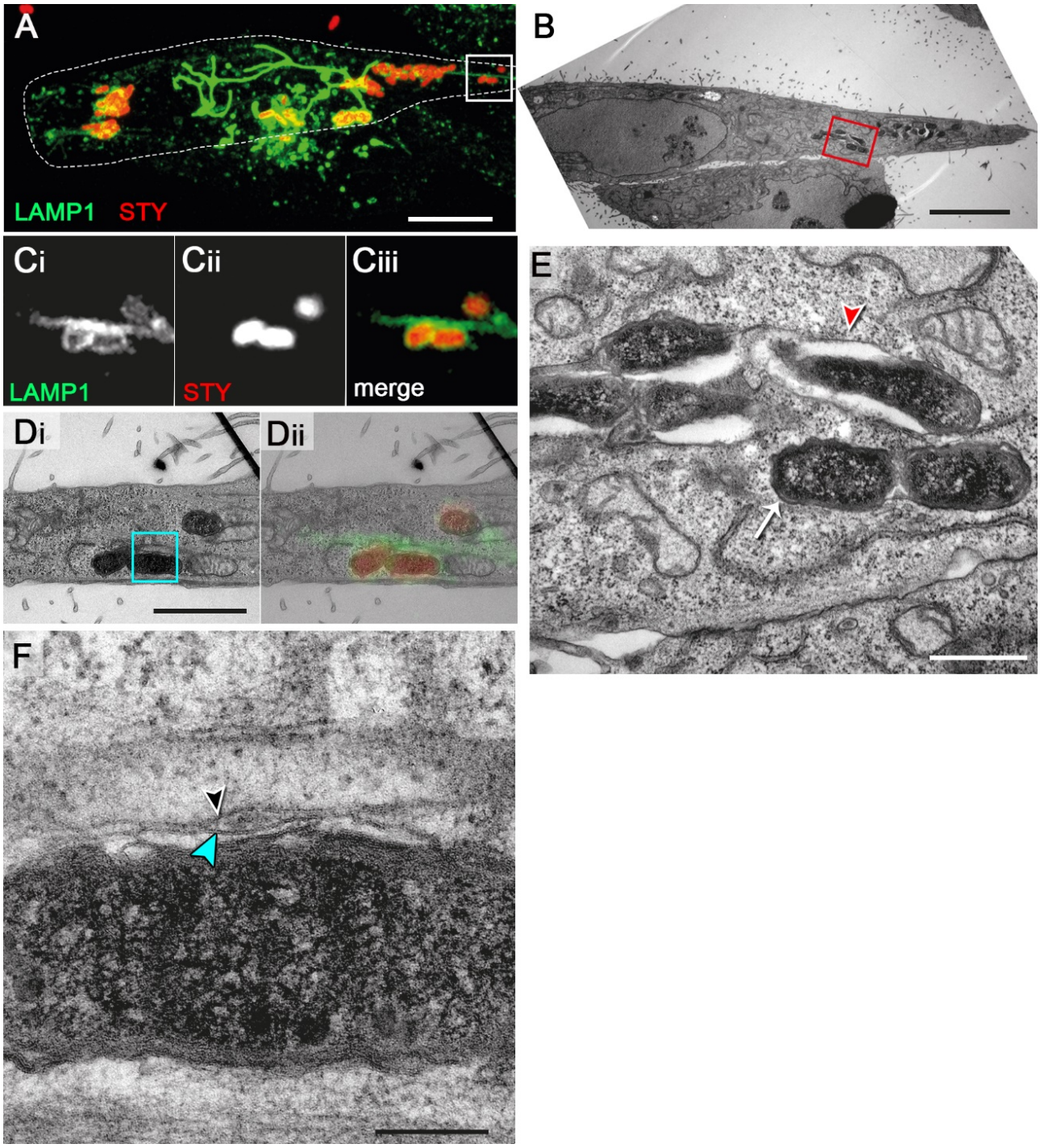

978

979 **Fig. S 4. CLEM of intracellular STM.** HeLa cells expressing LAMP1-GFP (green) were
980 infected with STM WT expressing mCherry (red). Cells were fixed 7 h p.i. and processed for
981 confocal microscopy (**A, C**) and TEM of ultrathin sections (**B, D, E, F, G**). **A**) An infected cell
982 showing a distinct LAMP1-GFP-positive SIF network was identified and further analyzed
983 (maximum intensity projection, MIP). **B)** TEM overview image of a host cell harboring several
984 salmonellae. **Ci, ii, iii, Di, ii**) For correlation, TEM and CLSM images were superimposed. **E**)

985 Detail of individual STM cells in SCV with single membrane (red arrowhead, white arrow). **F,**
986 **G**) Detail views of small sections of double membrane SIF with inner (black arrowhead) and
987 outer (blue arrowhead) membrane. Scale bars: 10 µm (**A**), 7 µm (**B**), 2 µm (**D**), 750 nm (**E**),
988 200 nm (**F**).
989

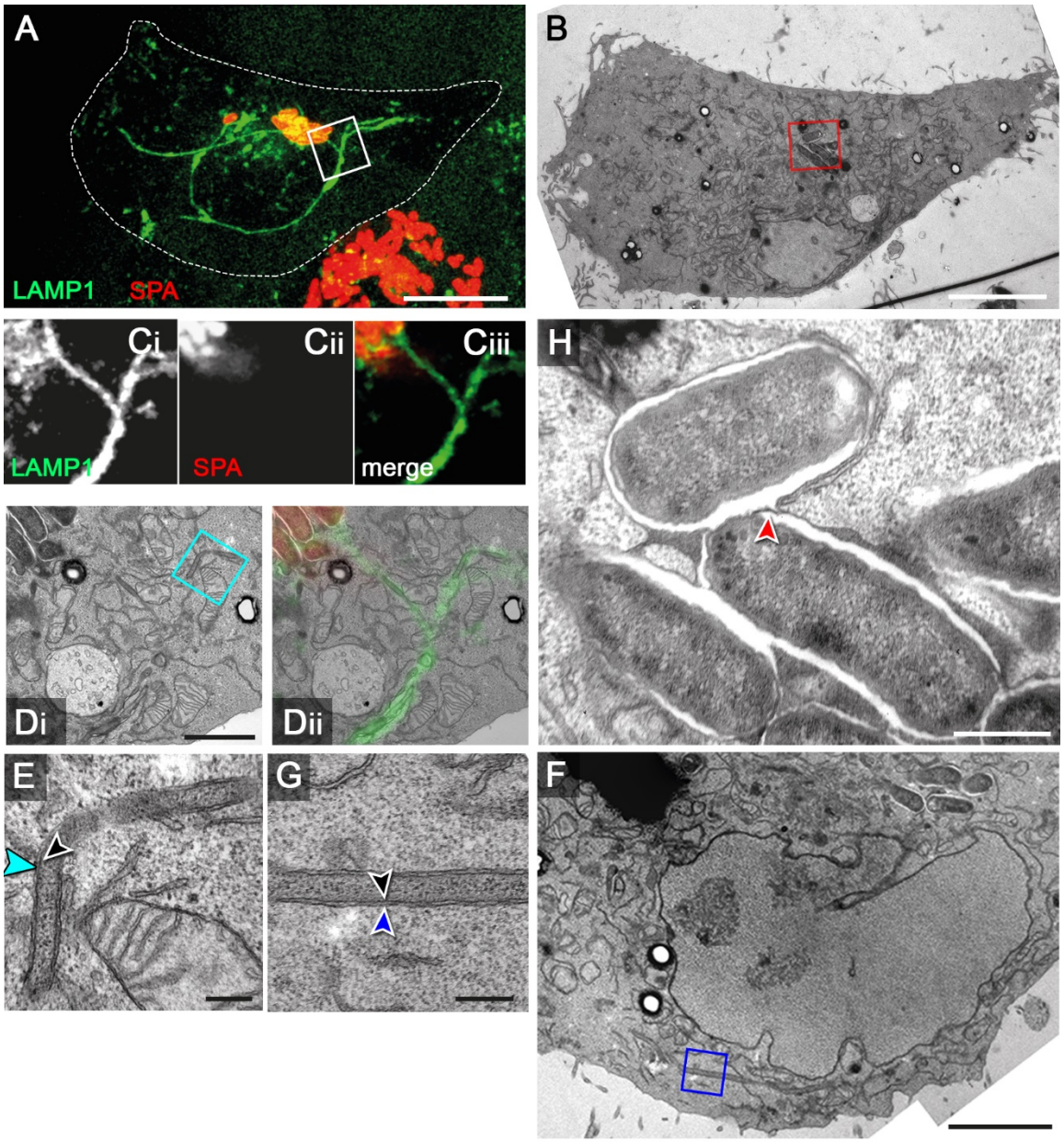

990

991 **Fig. S 5. CLEM of intracellular STY.** HeLa cells expressing LAMP1-GFP (green) were
992 infected with STY WT expressing mCherry (red). Cells were fixed 7 h p.i. and processed for
993 confocal microscopy (**A**, **C**) and TEM of ultrathin sections (**B**, **D**, **E**, **F**). **A**) An infected cell
994 showing a distinct LAMP1-GFP-positive SIF network was identified and further analyzed
995 (MIP). **B**) TEM overview image of a host cell harboring several salmonellae. **Ci**, **ii**, **iii**, **Di**, **ii**)
996 For correlation, TEM and CLSM images were superimposed. **E**) Detail of individual STY cells
997 in SCV with single membrane (red arrowhead, white arrow). **F**) Detail view of a small section

998 of a double membrane SIF with inner (black arrowhead) and outer (blue arrowhead) membrane.

999 Scale bars: 10 μm (**A**), 7 μm (**B**), 2 μm (**D**), 750 nm (**E**), 200 nm (**F**).

1000

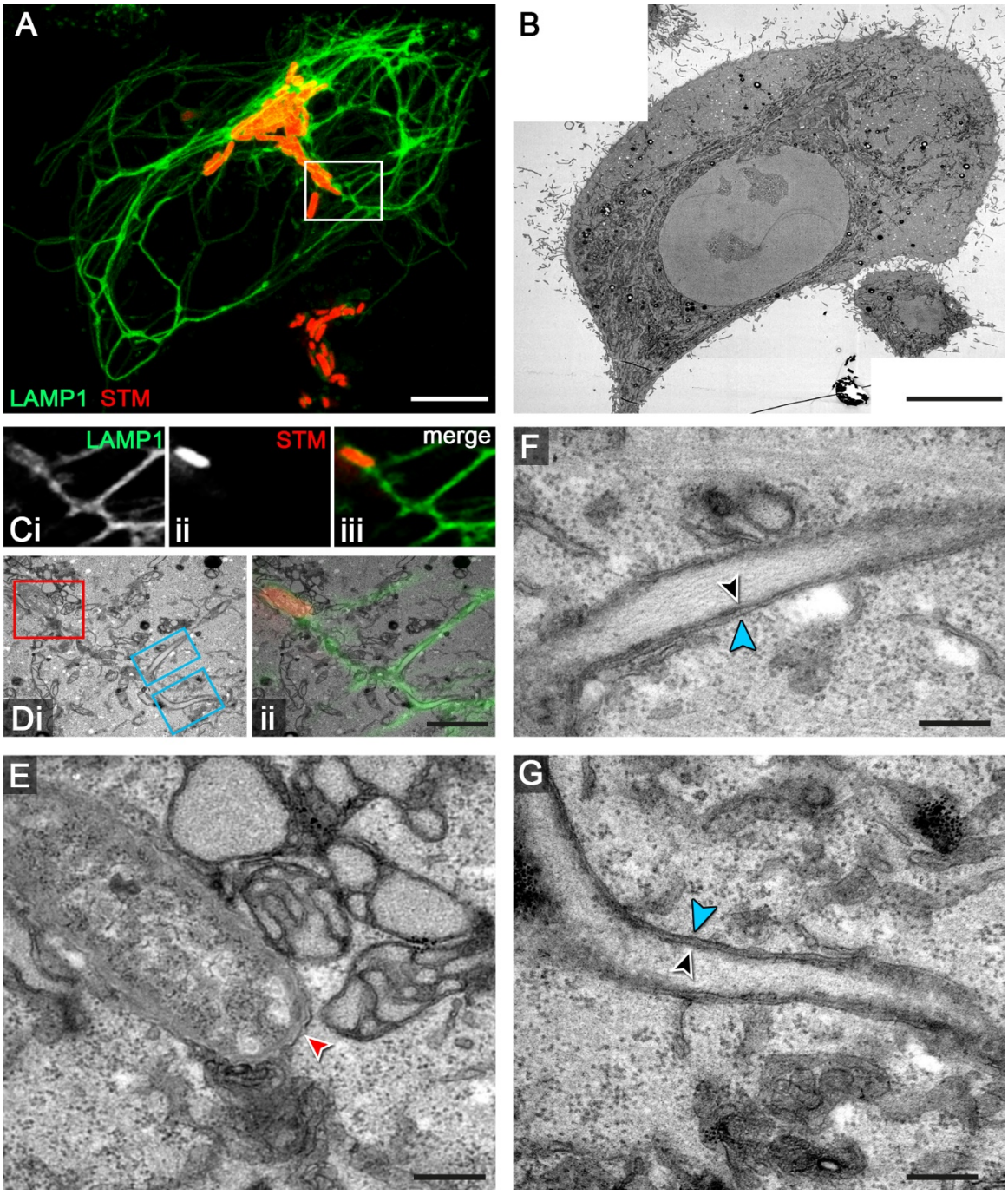

Fig. S 6. CLEM of intracellular SPA. HeLa cells expressing LAMP1-GFP (green) were infected with SPA WT expressing mCherry (red). Cells were fixed 7 h p.i. and processed for confocal microscopy (**A**, **C**) and TEM of ultrathin sections (**B**, **D**, **E**, **F**, **G**, **H**). **A**) An infected cell showing a distinct LAMP1-GFP-positive SIF network was identified and further analyzed (MIP). **B**) TEM overview image of a host cell harboring several salmonellae (red box). **Ci**, **ii**, **iii**, **Di**, **ii**) For correlation, TEM and CLSM images were superimposed. **H**) Detail of individual

SPA cells in SCV with single membrane (red arrowhead). **D**, **F**) Overviews showing SIF distal to the SCV, regions shown in details are indicated by light or dark blue boxes. **E**, **G**) Corresponding detail views of double membrane SIF with inner (black arrowhead) and outer (light blue, dark blue arrowheads) membranes. Scale bars: 10 µm (**A**), 7 µm (**B**), 2 µm (**D**), 250 nm (**E**, **G**), 3 µm (**F**), 500 nm (**H**).

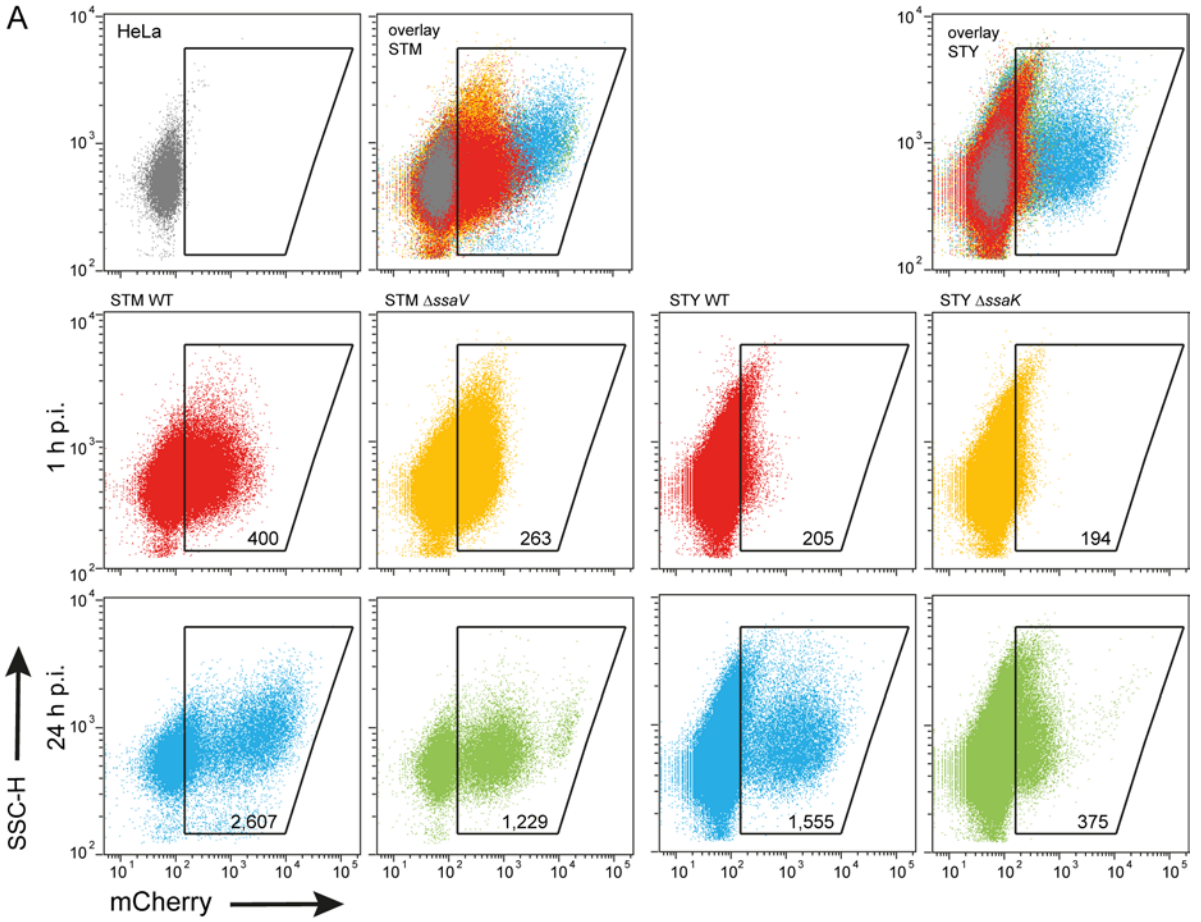

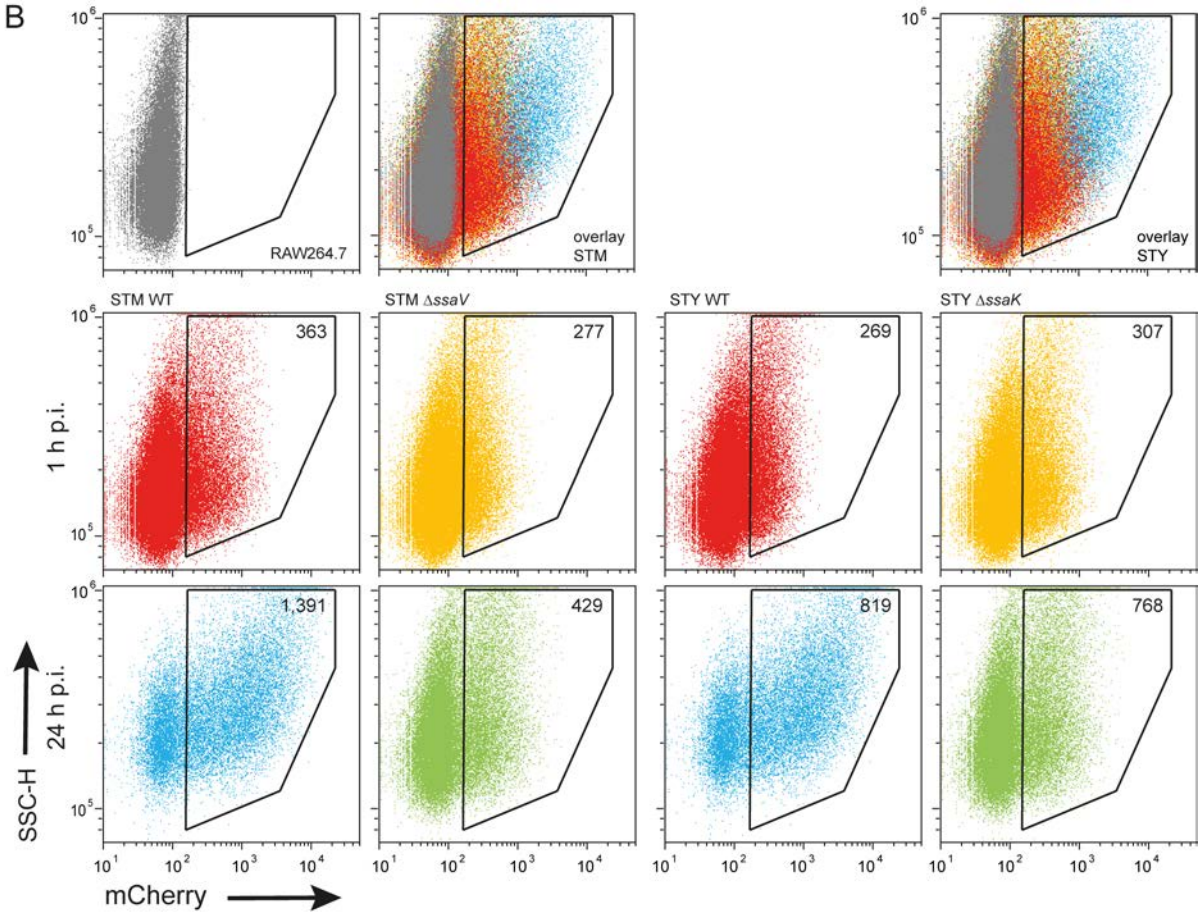

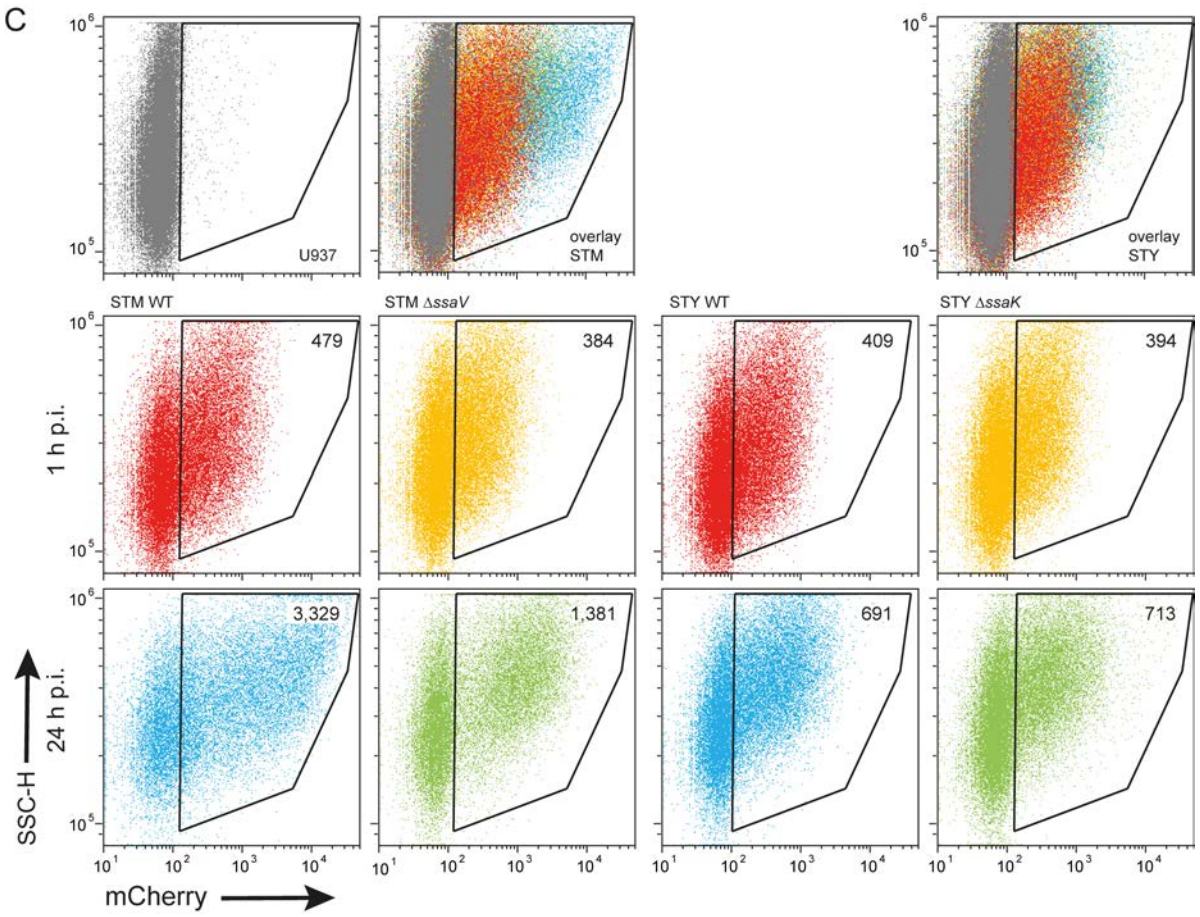

1017

1018 **Fig. S 7. Intracellular proliferation of STM and STY determined by flow cytometry.** The
1019 single dot plots of the experiment shown in **Fig. 8** are displayed. HeLa cells (**A**), RAW264.7
1020 macrophages (**B**), or U937 macrophages (**C**) were used as host cells. Gating for infected host
1021 cells was made using non-infected cells (grey dots) as control. Overlays of dot plots show WT
1022 *Salmonella* at 1 h or 24 h p.i. in red and blue, respectively, and Δ*ssaV* or Δ*ssaK Salmonella* at
1023 1 h or 24 h p.i. in orange and green, respectively. The X-mean values for mCherry fluorescence
1024 intensities of infected cells are indicated the gates for infected host cells. Assays were
1025 performed in three biological replicates, one representative replicate is shown.